Check for updates

Sixty years of electrochemical optical spectroscopy: a retrospective

Chao-Yu Li [ab] and Zhong-Qun Tian *[a]

Sixty years ago, Reddy, Devanatan, and Bockris performed the first *in situ* electrochemical ellipsometry experiment, which ushered in a new era in the study of electrochemistry, using optical spectroscopy. After six decades of development, electrochemical optical spectroscopy, particularly electrochemical vibrational spectroscopy, has advanced from a phase of immaturity with few methods and limited applications to a phase of maturity with excellent substrate generality and significantly improved resolutions. Here, we divide the development of electrochemical optical spectroscopy into four phases, focusing on the proof-of-concept of different electrochemical optical spectroscopy studies, the emergence of plasmonic enhancement-based electrochemical optical spectroscopic (in particular vibrational spectroscopic) methods, the realization of electrochemical vibrational spectroscopy on well-defined surfaces, and the efforts to achieve *operando* spectroelectrochemical applications. Finally, we discuss the future development trend of electrochemical optical spectroscopy, as well as examples of new methodology and research paradigms for *operando* spectroelectrochemistry.

1. Introduction

Since the nineteenth century, the electrochemical research method has been developed mainly by using electric signals

[a] *State Key Laboratory of Physical Chemistry of Solid Surfaces, College of Chemistry and Chemical Engineering, Xiamen University, Xiamen 361005, China.*
E-mail: zqtian@xmu.edu.cn
[b] *School of Materials Science and Engineering, Tongji University, Shanghai, 201804, China*

as excitation and detection means, *i.e.*, to study the structure and reaction mechanism at electrode/electrolyte interfaces, with precise measurement of current, potential and charge (*e.g.*, chronoamperometry, chronopotentiometry, cyclic voltammetry, AC impedance, *etc.*).[1–4] The electrochemical methods developed with the advances in electronics have now achieved a very high detection sensitivity, capable of detecting a change in a sub-monolayer of atoms or molecules (*i.e.*, the adsorption/desorption of a sub-monolayer of molecules on a single crystal electrode surface).[1–4] However, the traditional electrochemical

Chao-Yu Li

Chao-Yu Li is a professor at School of Materials Science and Engineering, Tongji University, China. He obtained his PhD degree in physical chemistry from Xiamen University in 2016. And then, he carried out postdoctoral research at Massachusetts Institute of Technology and Emory University in the U.S.A, respectively. He joined Tongji University in 2023, and his main research interests include spectro-electrochemistry, electrochemical energy storage and conversion, plasmonics, and single-molecule spectroscopy, etc.

Zhong-Qun Tian

Zhong-Qun Tian is a full professor of chemistry at Xiamen University. He obtained his BSc degree from Xiamen University in 1982 and completed his PhD under the supervision of Prof. Martin Fleischmann at University of Southampton in 1987. Prof. Tian is a member of the Chinese Academy of Sciences, a Fellow of the Royal Society of Chemistry and the International Society of Electrochemistry, and served as President of the International Society of Electrochemistry from 2019 to 2020. His main research interests include SERS, spectroelectrochemistry, nanochemistry, plasmonics, and catassembly, etc.

This journal is © The Royal Society of Chemistry 2024

Chem. Soc. Rev., 2024, **53**, 3579–3605 | 3579

Table 1 Four phases in the development of electrochemical optical spectroscopy and related key spectroscopic techniques

Development Phase	Spectroscopic technique	Year	Spectroscopic mode	Electrochemical system	Features and notes
Phase I (proof-of-concept of electrochemical optical spectroscopies)	EC-ellipsometry[7]	1963	Normal	Anodic formation of Hg_2Cl_2 films on Hg electrodes	First in situ electrochemical optical spectroscopy. Due to the limited detection sensitivity of instrument, the film electrode with a certain thickness containing a significant number of analytes is highly desirable and decisive.
	EC-UV-Vis[8]	1964	Normal	Electro-redox of ferrocyanide and chronopotentiometric electrooxidation of o-tolidine	First in situ spectroscopic study of electrochemical product in solution phase. The analytes need to absorb light in UV-Vis wavelength.
	EC-IR[9]	1966	ATR-based	Electroreductions of 8-quinolinol and tetramethylbenzidine free radicals.	First in situ spectroelectrochemistry using vibrational spectroscopy, in which Ge was used simultaneously as a working electrode and a waveguide for multi-internal reflection.
	EC-SHG[10]	1967	Normal	Electrified Si and Ag electrodes.	First in situ nonlinear spectroscopy at the electrochemical interface.
	EC-Raman[11]	1973	Normal	Electrochemical deposition of Hg_2Cl_2, Hg_2Br_2, and HgO.	Hg_2Cl_2, Hg_2Br_2, and HgO, the same systems studied by Bockris in the first EC-ellipsometry, are strong Raman scatters, which facilitate the normal Raman measurement (external reflection) and also the optimization of the optic configuration and cell.
	EC-IR using external reflection[12,13]	1980	Normal	Electrooxidation of thianthrene and the adsorption of indole and H_2O on Pt electrodes.	An external-reflection mode was used for the first time to acquire IR absorption signals of molecules adsorbed at the electrode surface.
	EC-SFG[14]	1990	Normal	Adsorption of CO and CN^- on the Pt electrode surface.	First in situ nonlinear spectroscopy with molecular vibrational information at the electrochemical interface.
Phase II (plasmonic enhancement-based electrochemical vibrational spectroscopies)	EC-SERS[15,16]	1974-1977	Nanostructure-based	Adsorption of pyridine on an electrochemically roughened Ag electrode surface	The discovery of SERS, in which the surface enhancement effect enables the high-quality Raman spectroscopic measurement of (sub)monolayer of molecules adsorbed on the electrode surface.
	EC-SERS on TMs[17-20]	1987	Nanostructure-based	EC-SERS on different TM layers (i.e., Fe,[20] Ni,[17] Co,[17] Pt,[18] Pd,[18] and Pb,[19] etc.) deposited on Au or Ag substrates	A strategy of "borrowing" high SERS activity from highly SERS-active Au or Ag substrates to probe the Raman signal on SERS-weakly or non-SERS-active TM surfaces.
	EC-SERS with self-assemble monodisperse colloids[21]	1995	Nanostructure-based	EC-SERS on monodisperse Au or Ag nanoparticles assembled on organosilane-polymer-modified solid substrate	For the first time, the monodisperse high-SERS active nanoparticles were regularly arranged on the substrate for desirable SERS activity with good stability and reproducibility.
	EC-SEIRAS[22-25]	Mid-1990s	Nanostructure- and ATR-based	Adsorption of AQ-COOH,[22] water,[23] water-sulfate,[24] and pyridine[25] on thin Ag or Au film electrodes.	Molecules on evaporated thin metal films exhibit enormously strong IR absorption; however, the enhancement factor of SEIRAS is modest compared to that of SERS. The vacuum evaporation rate or electrochemical deposition rate to prepare the metal film electrode are crucial to the enhancement.
Phase III (electrochemical vibrational spectroscopies on well-defined surfaces)	EC-IR on single-crystal electrode[26-28]	Late 1980s	ATR-based	Adsorption of CO[26,27] and hydrogen[28] at Pt single-crystal electrodes	The external-reflection spectroscopic mode promotes the vibrational spectroscopy on a well-defined electrode surface. SPP induced by ATR configuration enhance the Raman signal on atomically flat electrode surfaces.
	EC-Raman on single-crystal electrodes[29,30]	1991;[29] 1998[30]	ATR-based	Adsorption of pNDMA at Ag single-crystal electrodes;[29] adsorption of pyridine at Cu single-crystal electrodes[30]	
	EC-SFG on single-crystal electrode[31,32]	1994	Normal	Adsorption of hydrogen[31] and cyanide[32] at Pt single-crystal electrodes	
	EC-SHINERS[33]	2010	Nanostructure-based	Adsorption of hydrogen at Pt single-crystal electrodes	The ultra-thin, pinhole-free dielectric shell of SHIN plays the key role.

3580 | Chem. Soc. Rev., 2024, 53, 3579–3605

This journal is © The Royal Society of Chemistry 2024

Table 1 (continued)

Development Phase	Spectroscopic technique	Year	Spectroscopic mode	Electrochemical system	Features and notes
	EC-TERS[34,35]	2015	Tip-based	Protonation and deprotonation of 4-PBT on Au single-crystal electrodes;[34] electrochemical redox of Nile blue on an ITO electrode.[35]	The electrochemistry, plasmon-enhanced spectroscopy, and SPM with high spatial resolution are combined to enable vibrational spectroscopy on well-defined electrodes.
	EC-nano FTIR[36]	2019	Tip-based	Potential-dependent aggregations of sulfate and ammonium at the graphene-electrolyte interface.	
Phase IV (operando electrochemical vibrational spectroscopies)	Operando EC-IR[37] and EC-Raman[38,39]	Early 2010s	Normal	EC-IR of the adsorbed CO on the Pt membrane electrode in an operating fuel cell;[37] EC-Raman of water distribution in Nafion membranes at various hydration states in operating fuel cells.[38,39]	The design of cells compatible with operando spectroscopic experiments is essential, and the normal external-reflection spectroscopic mode is suitable under real working conditions. Normally, the exterior of the cell was changed to a transparent window, and the electrode component requires a hole to allow for the optic access.
	Operando fiber-based EC-Raman[40]	2016	Fiber-based	Operando study of electrolyte distribution inside a laminate cell.	Without using a transparent optic window in place of the battery exterior, optic fibers can be used as small probes embedded directly into the practical or commercial batteries for non-destructive analysis of the electrolytes during cycling. Normally, silicon and TAS are used as fiber materials for Raman and IR, respectively.
	Operando fiber-based EC-IR[41]	2022	Fiber-based	Electrolyte analysis in a commercial 18650 jelly roll and a Swagelok cell.	

Abbreviations: EC-IR, electrochemical infrared spectroscopy; EC-SHG, electrochemical second hormonic generation; EC-SFG, electrochemical sum frequency generation; EC-SERS, electrochemical surface-enhanced Raman spectroscopy; EC-SEIRAS, electrochemical surface-enhanced infrared absorption spectroscopy; TERS, tip-enhanced Raman spectroscopy; TMs, transition metals; TM-coated Au, transition metal-coated Au; EC-SHINERS, electrochemical shell-isolated nanoparticle-enhanced Raman spectroscopy; SHIN, shell-isolated nanoparticle; EC-nano FTIR, electrochemical Fourier transform infrared nano-spectroscopy; AQ-COOH, 2-anthraquinonecarboxylic acid; pNDMA, para-nitrosodimethylaniline; 4-PBT, (4'-[pyridin-4-yl]biphenyl-4-yl)methanethiol; SPP, surface plasmon polariton; SPM, scanning probe microscopy; TAS, $Te_2As_3Se_5$. Both operando fiber-based EC-Raman and EC-IR refer to operando spectroscopic experiments in batteries.

methods have their intrinsic limitations; for instance, the electrical signal is incapable of chemically recognizing specific molecules and revealing the bonding information and fine molecular structure of the individuals. Accordingly, to accurately identify various species on the electrode, and to explain the mechanism of electrochemical reaction, it is imperative to integrate other advanced technologies into the modern electrochemical methods, thus offering a great opportunity to apply optical spectroscopy in electrochemical studies.[5]

After sixty years of development, the main frame of the electrochemical optical spectroscopy has been established, moving forward from the early phase of proof-of-concept of spectroscopic methods to the phase of making practical contributions to the field of electrochemistry.[6] In particular, since 2010, the operando spectroscopic technique has attracted considerable attention because it allows for the real-time studies of the correlations between electrochemical performance with chemical and structural changes inside electrochemical devices under real working conditions, and this methodology, which advances the object of study from the previous ideal electrochemical interface to the practical interphase between the electrode and electrolyte (namely, "from the interface to the interphase"), has become an important application in spectroelectrochemistry. Therefore, it is necessary to review the history and different phases of the development of electrochemical optical spectroscopy (in this review, optical spectroscopy refers to the spectroscopy studies in the spectral wavelength range from ultraviolet to IR), and to discuss the new methodology and research paradigm for operando spectroelectrochemistry.

Here, as shown in Table 1, we divide the development into four phases, focusing on the proof-of-concept of different electrochemical optical spectroscopy studies (phase I), the emergence of plasmonic enhancement-based electrochemical vibrational spectroscopic methods (phase II), the realization of electrochemical vibrational spectroscopy on well-defined surfaces (phase III), and the development of operando electrochemical vibrational spectroscopy (phase IV).

2. Four phases of development of electrochemical optical spectroscopy

2.1. Phase I

2.1.1. Proof-of-concept of electrochemical optical spectroscopy studies. Phase I corresponds to the pioneering works establishing the proof-of-concept for electrochemical optical spectroscopy, as shown in Table 1. Between the 1960s and 1970s, electrochemists seized the opportunity provided by the rapid development of spectroscopy at that time, and established a number of electrochemical optical spectroscopy technologies.[5] In 1963, the first in situ electrochemical optical spectroscopy, that is, electrochemical ellipsometry (EC-ellipsometry) experiments, was reported by Bockris et al.[7] They kept the current constant while recording the changes in the intensity of the polarized light on the surface of the electrode

This journal is © The Royal Society of Chemistry 2024

Chem. Soc. Rev., 2024, **53**, 3579–3605 | **3581**
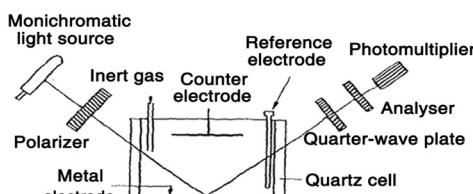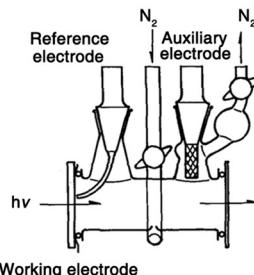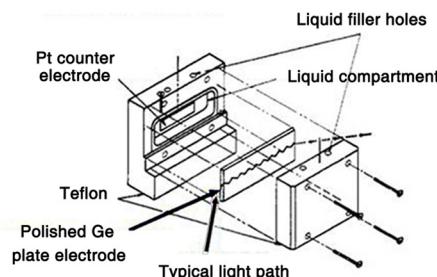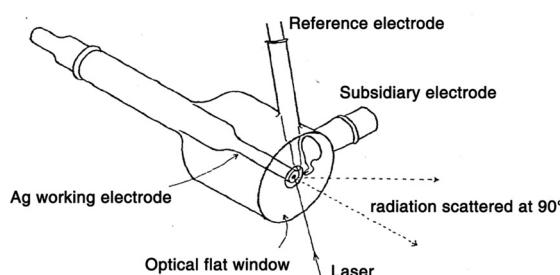
Fig. 1 Schematics of the electrochemical cell for the pioneering work of EC-ellipsometry (A), EC-UV-Vis (B), EC-IR (multi-internal reflection) (C), EC-Raman (D), EC-IR (external reflection) (E), respectively. Fig. 1A is reproduced with permission from ref. 7. Copyright 1963 Elsevier B.V. Fig. 1B is reproduced with permission from ref. 43. Copyright 1968. Elsevier B.V. Fig. 1C is reproduced with permission from ref. 9. Copyright 1966 American Chemical Society. Fig. 1D is reproduced with permission from ref. 15. Copyright 1974 Elsevier B.V. Fig. 1E is reproduced with permission from ref. 44. Copyright 1984 Elsevier B.V.

using an ellipsometer in real time (the method was referred to as "chronoellipsometry" in this work); the formation and growth mechanisms of the thin calomel film on the mercury electrode were *in situ* studied (see Fig. 1A for the electrochemical cell). However, ellipsometry spectroscopy requires a high degree of surface smoothness in the electrode material. Additionally, the bulk electrolyte phase affects the optical path during ellipsometry measurement when the excitation and collection angles are varied. Furthermore, it is challenging to differentiate between the optical changes induced by the adsorbed species and electronic changes on the electrode surface. At a Faraday Discussion meeting in the early 1970s, there was an intense discussion on the ionic and electronic contributions to the changes in reflectivity at Pt electrodes during hydrogen adsorption.[42] Therefore, a careful interpretation is required when analyzing reflectance results in the presence of specific adsorption.

It is important to note that due to the limited detection sensitivity of the instrument during the early stages of spectroelectrochemistry, a calomel film electrode with a certain thickness played a crucial role in validating the proof-of-concept of the new method because it contains a considerable number of molecules, which greatly facilitated the acquisition of optical signals on electrode.

In 1964, Kuwana *et al.* used a simple but classic optical spectroscopic technique, UV-Vis spectroscopy, in the electrochemical

system for the first time.[8] They used a common transmission optical configuration for UV-Vis measurement and a transparent tin dioxide as the working electrode (Fig. 1B). In this work, the electro-redox of ferrocyanide in a KCl solution and the chronopotentiometric electrooxidation of *o*-tolidine were recorded. As a milestone in the early stages of spectroelectrochemistry, this was the first time when the electrochemical reaction product in the solution phase was studied using a spectroscopic technique. It is worth noting that, in UV-Vis measurements, this method is mainly used for analytes that can absorb excitation wavelengths of light.

2.1.2. Electrochemical vibrational spectroscopy. Infrared (IR), Raman, and sum frequency generation (SFG) spectroscopy are currently the most widely used vibrational spectroscopic techniques in surface and material science.[5,45–48] Compared to UV-Vis absorption and conventional electrochemical techniques, one of the major advantages of vibrational spectroscopy is its high energy resolution for chemical recognition, *e.g.*, for Raman spectroscopy with an excitation wavelength in the visible spectral region, the spectral resolution can reach one wavenumber or even better (≤ 1 cm^{-1}), which corresponds to an energy resolution of around 0.1 milli-electron volts (meV).[49] This energy resolution is at least two orders of magnitude higher than that of conventional electrochemical techniques, and this advantage is also the reason why molecular vibrational spectroscopy is known as the finger-printing technique.

In 1966, a meaningful electrochemical infrared (EC-IR) experiment was conducted by Mark and Pons,[9] in which a polished semiconducting Ge plate was simultaneously used as a working electrode and a waveguide, enabling a multiple-reflection configuration of IR light (Fig. 1C). This is the first report of *in situ* electrochemical vibrational spectroscopy; however, it is worth noting that Ge is not a universal electrode material, and other electrode materials commonly used in the electrochemistry field, such as Au, Pt, and Pd, cannot be applied in the attenuated total reflectance (ATR)-IR mode, thus limiting the generality of this method at that time.

In 1973, Fleischmann *et al.* achieved an breakthrough in spectroelectrochemistry, that is, the application of Raman spectroscopy in the electrochemical study for the first time.[11] A prominent advantage of Raman spectroscopy compared to IR absorption is that Raman spectra can be recorded by using lasers in the visible wavelength region. Therefore, the absorption of incident light by the aqueous solution and the glass optical window is negligible. As a result, it is more convenient to use a generalized electrochemical cell for Raman spectroscopy measurements, for example, the incident light can be directed to the electrode surface through a glass optical flat and the aqueous electrolyte (the electrochemical cell is shown in Fig. 1D[15]). This is the first time that an external reflection excitation-collection mode has been used in electrochemical vibrational spectroscopy, which is more suitable for the use of a common rod-like metal electrode in spectroelectrochemistry and thus more attractive to the electrochemistry community.

It should be noted that, in the absence of the resonance effect and surface enhancement, the differential Raman cross-section is generally smaller than 10^{-29} cm^2 sr^{-1}, which is approximately 10 orders of magnitude lower than IR absorption, resulting in an extremely weak Raman signal.[50] Hence, back in 1972 when the authors discussed the possibility of obtaining Raman spectra from the electrode surface, the mercury/calomel system was recommended as calomel has an exceptionally large Raman scattering cross-section (*i.e.*, a strong Raman scatter).[44] At the same time, to generate a large-area mercury surface, thin films of Hg_2Cl_2 were formed on mercury droplets that had been electrodeposited onto a Pt disc foil.[11] As a result, a characteristic Hg–Hg stretch band at 168 cm^{-1} was observed, which disappeared upon shifting the potential to a more cathodic state, indicating that the signal originated from the electrode surface layer. Furthermore, similar observations were obtained with the Hg_2Br_2 and HgO system, suggesting for the first time that Raman scattering could be employed for *in situ* spectroelectrochemical studies.[11,44]

It is of significance that this mercury oxide and halide system is the same system which Bockris *et al.* studied ten years ago for the first *in situ* electrochemical ellipsometry measurement (1963),[7] in which the excellent optical scatters facilitate the collection of spectroelectrochemical signals, the optimization of optical path, and the design of electrochemical Raman (EC-Raman) spectroscopic cells. However, given the larger number of molecules in the mercury oxide and halide system, it was still highly desirable to realize investigations of (sub-)monolayer adsorption (reaction) species on the electrode surface, which are more significant and more challenging. In practical terms, this means that the research object needs to be advanced from the film electrode studied in the early work to more important interfaces, such as the electrode/electrolyte interface, which requires a much higher detection sensitivity.

In 1980, a significant work was conducted by Bewick *et al.*,[12,13] in which an external-reflection mode was used for the first time to acquire IR absorption signals at the electrode surface. Based on this configuration, a commonly used Pt disc-shaped electrode served as a working electrode to study the hydrogen and water adsorption on the Pt surface under potential modulations (Fig. 1E and 2A). Notably, to avoid the significant absorption of IR light by the electrolyte, a thin-layer
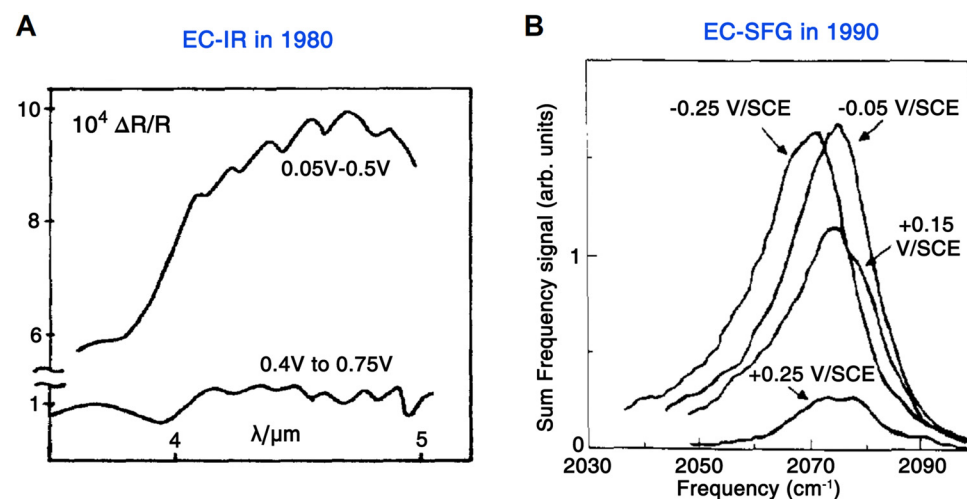
Fig. 2 (A) First EC-IR measurement using an external-reflection mode by Bewick *et al.* in 1980, in which the spectra were recoded from the Pt/1 M H$_2$SO$_4$ interface under potential modulations. (B) First EC-SFG spectroscopy study by Tadjeddine *et al.* in 1990. These SFG spectra were obtained from CO adsorbed on a Pt electrode. Fig. 2A is reproduced with permission from ref. 12. Copyright 1980 Elsevier Ltd. Fig. 2B is reproduced with permission from ref. 14. Copyright 1990 Elsevier B.V.

This journal is © The Royal Society of Chemistry 2024

Chem. Soc. Rev., 2024, 53, 3579–3605 | 3583

electrolyte between the electrode surface and window was required. At the same time, the authors employed a continuous potential modulation method to improve the signal-to-noise ratio. This method was called electrochemically modulated infrared spectroscopy (EMIRS),[51] which is the first electrochemical IR technique of using an electrode potential difference strategy.[52]

In the meantime, with short laser pulses, nonlinear optics started to play an important role in spectroelectrochemistry. Compared with IR and Raman spectroscopic methods, nonlinear spectroscopis methods, such as sum frequency generation (SFG) and second harmonic generation (SHG) are characterized by their inherent surface specificity and sensitivity.[47] In 1967, Lee *et al.* reported the first electrochemical SHG measurements, in which the second-harmonic reflected light was *in situ* detected on electrified silicon and silver surfaces in KCl solutions.[10] SFG ($\omega_{SFG} = \omega_1 + \omega_2$) is an extension of the SHG process ($\omega_1 = \omega_2 = \omega$, $\omega_{SHG} = 2\omega$), and in addition to having the high sensitivity of the SHG technique, SFG is also capable of probing the characteristic vibrational transitions of molecules.[47]

SFG spectroscopy has several distinct advantages over Raman scattering and IR absorption spectroscopy: (1) under the electric dipole approximation, SFG is only allowed in media with a broken centrosymmetry, making it an inherently surface specific spectroscopic technique; (2) at the interface of a molecule adsorbed on a metal, SFG can probe the response of the adsorbed molecule, electronic excitations of the metal, and the interaction of molecule adsorption modifying the density of states at the interface; (3) in cases involving short pulsed lasers,

SFG is able to investigate the vibrational dynamics at the interface with a time resolution from nanosecond (ns) to less than 100 femtosecond (fs) and (4) the surface structure can be studied through anisotropy experiments, among other techniques.[47,53–56]

In 1987, in order to obtain the fingerprint vibrational spectroscopic information at the interface, Shen *et al.* developed IR-visible SFG spectroscopy, where one incident light source is a tunable IR laser and the other incident light source is a visible laser with a fixed wavelength, *i.e.*, the IR pulse spatially and temporally overlaps with a visible pulse for the SFG signal.[57–59] Three years later (1990), Guyot-Sionnest and Tadjeddine applied SFG spectroscopy to electrode–electrolyte interfaces for the first time.[14] Because an IR beam is used as one of the excitations, a similar issue to that in EC-IR spectroscopy, *i.e.*, the strong adsorption of IR light by electrolyte, should be tackled. Therefore, a thin-layer cell similar to the one commonly used in EC-IR spectroscopy was adopted in electrochemical sum frequency generation (EC-SFG) measurements to study the adsorption of CO, CN^-, and SCN^- anions on Pt electrodes. As shown in Fig. 2B, no background interference from the electrolyte or Pt electrode was observed in the SFG signal of the CO stretching vibration (*i.e.*, a well-defined resonance of vibration over an unobservable contribution from metal), demonstrating the characteristic surface sensitivity of EC-SFG, which is crucial and invaluable for studying adsorbed species on the electrode surface.

Electrochemical vibrational spectroscopy, including EC-IR, EC-Raman, and EC-SFG, among others, is characterized by its ability to provide fingerprint vibrational information from the
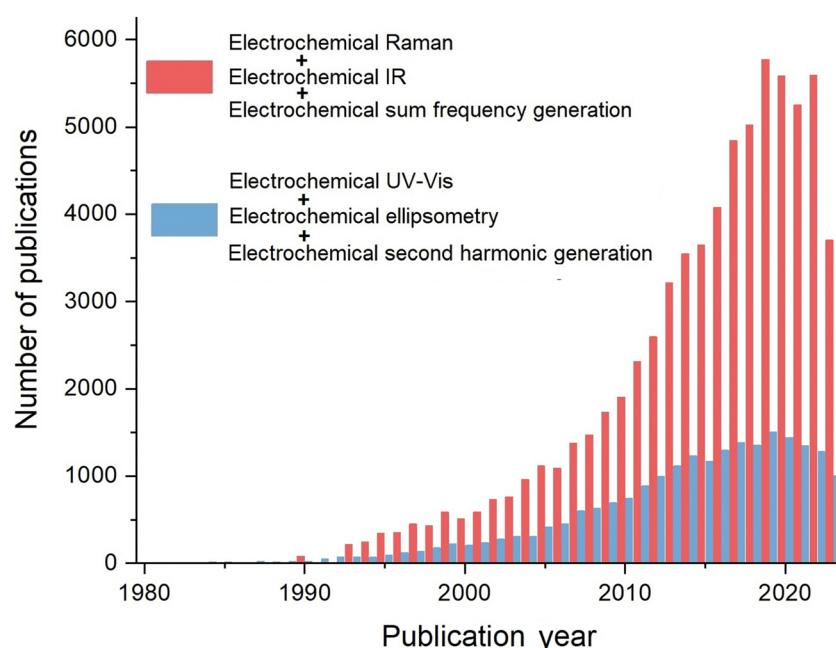
Fig. 3 The total number of articles on electrochemical vibrational spectroscopy methods using the key words "electrochemical Raman", "electrochemical IR", and "electrochemical sum frequency generation", and the total number of articles on other electrochemical optical spectroscopies using the keywords "electrochemical UV-Vis", "electrochemical ellipsometry", and "electrochemical second harmonic generation", respectively. These data are obtained through Web of Science®.

3584 | *Chem. Soc. Rev.*, 2024, **53**, 3579–3605

This journal is © The Royal Society of Chemistry 2024

electrochemical interface or bulk phases. Furthermore, the significant advancements in nanoscience since the 1990s have led to an explosive growth of electrochemical vibrational spectroscopic research studies, which has promoted the important new development phases of spectroelectrochemistry. A search was conducted through Web of Science® using the key words 'electrochemical Raman', 'electrochemical IR', 'electrochemical sum frequency generation', 'electrochemical UV-Vis', 'electrochemical second harmonic generation', and 'electrochemical ellipsometry', respectively. As revealed in Fig. 3, in recent years, the number of research articles on electrochemical vibrational spectroscopic methods (including Raman, IR, and SFG) is nearly 6000 per year, which is almost 4 times of the total number of articles on EC-ellipsometry, EC-SHG, and EC-UV-Vis. Therefore, the significant and rapid growth of electrochemical vibrational spectroscopy have notably contributed to phases II to IV in the development of electrochemical optical spectroscopy.

Herein, it is reasonable to present a comprehensive overview of the development of electrochemical optical spectroscopy methods, but with an emphasis on vibrational spectroscopy in light of historical and future development trends.

2.2. Phase II

2.2.1. Plasmonic enhancement-based electrochemical vibrational spectroscopy. In phase I, for the proof-of-concept, most electrochemical optical spectroscopic techniques used a normal external-reflection configuration (namely, the normal mode, as shown in Fig. 4A). However, the normal spectroscopic mode typically lacks high detection sensitivity (especially EC-Raman), so it is usually unsuitable to study small amounts of surface or interfacial molecules, let alone the active atomic sites. In phase II, to enhance the surface detection sensitivity, researchers have discovered and explored the surface enhancement effects based on plasmon resonance-active substrates, including electrochemically roughened substrates, nanoparticles, ordered nanostructures, nanoisland structures (*e.g.*, the thin metal films normally used in an ATR configuration), *etc.*, which can significantly improve sensitivity (Fig. 4B and C).[60,61]

2.2.2. EC-SERS. Compared to IR and SFG spectroscopy, Raman spectroscopy has prominent advantages in electrochemical system research due to the smaller interference from aqueous solution and the absence of special requirements for sample and electrochemical cell materials (for example,

quartz/glass can be used as the optical window).[45] However, as normal Raman scattering is a second-order process, the Raman signals are usually very weak. For a non-resonant molecule, the differential Raman cross-section is usually only (or below) 10^{-29} cm^{-2} sr^{-1}, and $10^{6\sim9}$ photons are needed to produce a Raman photon.[50] When Raman spectroscopy is used to detect the surface monolayer species, the corresponding Raman signal intensity is generally less than 1 photon count per second (*e.g.*, the strongest Raman peak of pyridine adsorbed on a mechanically polished Ni electrode is only $\sim$0.4 counts per second[45]). Therefore, these intrinsic limitations made it nearly impossible to study the surface adsorptions or reactions using Raman spectroscopy. However, it was in the brave attempt to challenge this impossible goal that SERS, demonstrating an extremely high surface sensitivity, was discovered.

In 1974, in order to overcome the extremely low detection sensitivity for surface adsorbed species in Raman spectroscopy, Fleischmann, Hendra, and McQuillan came up with a strategy to significantly increase the number of surface molecules, in which pyridine (Py) was chosen because of its very large Raman cross-section.[15] They used potential-controlled oxidation and reduction cycles (ORC) to increase the surface area of a silver electrode in an aqueous 0.1 M KCl electrolyte containing 0.05 M Py. As shown in Fig. 5, by using a front-reflection cell (see Fig. 1D for the schematic of cell), the Raman spectra obtained on the electrochemically roughened silver electrode exhibit unexpectedly high quality, and the distinct potential dependence suggested that the Raman signal originates from the electrode surface-adsorbed species. In fact, the preliminary result of this work was briefly introduced during a general discussion at the conference of 56th Faraday Discussions in 1973,[42] but it was formally published in 1974.[15]

In retrospect, although Fleischmann and co-authors were unaware of the SERS effect at the time, this work was the first SERS measurement, *i.e.*, EC-SERS (Fig. 5). They initially believed that the electrochemical roughening largely increased the electrode surface area and thus the number of surface adsorbed molecules, resulting in the acquisition of strong Raman signals from the surface adsorbed Py. With careful calculations and experimental verifications, Van Duyne and Jeanmaire found that the major contribution to the strong Raman signal intensity of adsorbed Py species is an anomalous enhancement of 5 to 6 orders of magnitude compared to those predicted from the scattering cross-section for Py in bulk.[16]
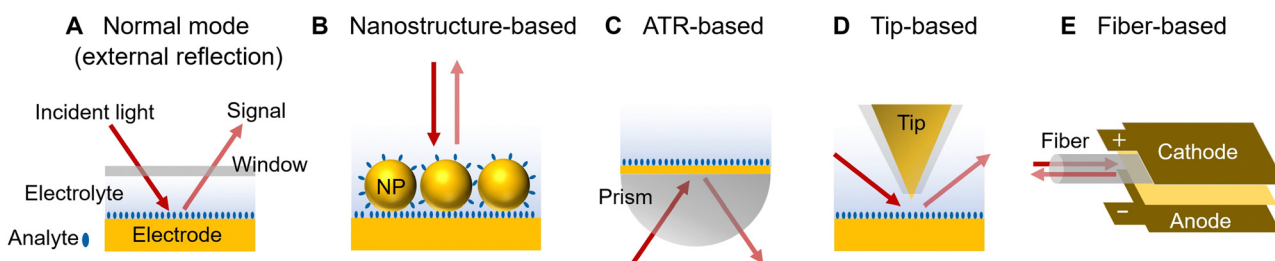

Fig. 4 Different electrochemical vibrational spectroscopic modes. (A) Normal mode (external reflection). (B) Nanostructure-based mode. NP is an abbreviation for nanoparticle. (C) ATR-based mode. (D) Tip-based mode. (E) Fiber-based mode.

This journal is © The Royal Society of Chemistry 2024

Chem. Soc. Rev., 2024, **53**, 3579–3605 | **3585**

EC-SERS in 1974
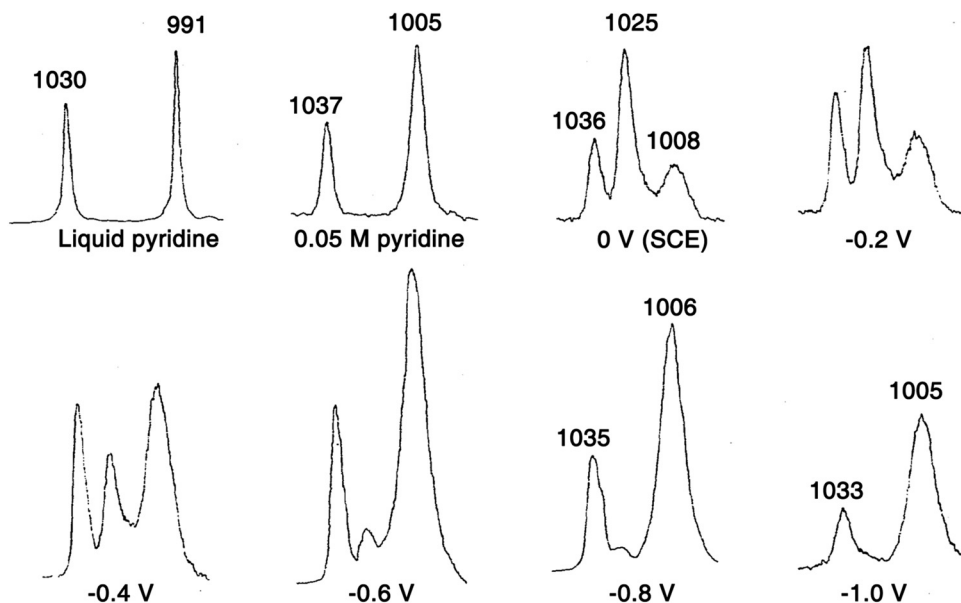
Fig. 5 First SERS experiment by Fleischmann *et al.* in 1974, in which the adsorption of pyridine was studied on a roughened Ag electrode surface. Reproduced with permission from ref. 15. Copyright 1974 Elsevier B.V.

However, their paper went through a long and exhaustive reviewing procedure and was eventually published in 1977.[16] In the same year, Albrecht and Creighton independently reported a similar result.[62] These pioneers presented strong evidence to demonstrate that the enormously strong surface Raman signals must be caused by a genuine enhancement of the Raman scattering efficiency itself. This Raman enhancement effect was later named SERS.[63,64]

The discovery of SERS created a sensation in the fields of surface science and spectroscopy;[50,65] after comprehensively studying the SERS effect through experiments and theorical calculations, people realized the enhancement is largely owing to the excitation of surface plasmon resonance (SPR).[66–70] In 1978, Moskovits proposed that the Raman enhancement in SERS is caused by the resonances of conduction electrons on the surface of roughened metal.[70] Moreover, he predicted that the Raman enhancement could be realized on Au, Ag, and Cu colloids. In 1979, Creighton *et al.* conducted the first study of SERS using Ag and Au colloids, which were synthesized through wet-chemical methods.[69]

Looking back at the history of SERS, the enthusiasm in the fields of surface science and electrochemistry was greatly motivated after the discovery of SERS, but soon wore off in the late 1970s. The main reasons are the limitations on the substrate material and morphology of SERS.[71] First, the generality of materials is limited to a few "free-electron like" metals, such as Au, Ag, and Cu.[72] However, the application of SERS on other electrode materials important to electrochemistry, such as weakly SERS-active or SERS-inactive group VIIIB transition metals (TMs), was difficult.

Therefore, a strategy of "borrowing" high SERS activity from highly SERS-active Au or Ag substrates was initially proposed by Van Duyne to study the adsorbates on semiconductor electrode surfaces, *i.e.*, n-GaAS(100), in 1983.[73] But in this method, the analytes were able to adsorb on the Ag surface as well, which may result in mixed signals from molecules adsorbed on both the semiconductor and Ag. In 1987, the Fleischmann group[17,20] and Weaver group[18,19] independently developed the "borrowing" strategy by coating a layer of different TMs, such as Fe,[20] Ni,[17] Co,[17] Pt,[18] Pd,[18] Pb,[19] *etc.* onto the surface of Au or Ag substrates. It is worth noting that the thickness of the coating layer of TMs should be kept as thin as possible to prevent the decay of the electromagnetic field transmitting through the layer, thus "borrowing" stronger plasmonic enhancement from the Au core. In 2002, utilizing the under potential deposition (UPD) and redox replacement methods, the well-controlled ultra-thin (as thin as a single atomic layer) and pinhole-free Pt-group metal layer-coated Au nanoparticle-dispersed electrodes were developed by Weaver *et al.*, enabling a strong SERS signal on weakly SERS-active TM surfaces by "borrowing" the enhancement from the highly SERS-active Au nanoparticle core.[74]

In 2004, Tian *et al.* proposed an alternative "borrowing" SERS activity strategy through which monodispersed Au core-TM shell nanoparticles (Au@TM) can be directly prepared *via* wet-chemical methods.[75–77] In these methods, the material of TM shells can be changed from Pt to Pd, Ni, Rh, Ru, and Co, respectively; meanwhile, the monodispersed Au@TM nanoparticles can be conveniently drop cast onto the electrode surface, thereby facilitating the generalized spectroelectrochemical study.[71]

3586 | *Chem. Soc. Rev.*, 2024, **53**, 3579–3605

This journal is © The Royal Society of Chemistry 2024

The another major limitation of SERS is that SERS was predominantly used to study the molecules adsorbed on the nanostructure-based ill-defined substrate surfaces, such as roughened electrodes[15–20,73] or metal colloids;[69,78] however, it was challenging to carry out EC-SERS on well-defined or well-ordered electrode surfaces. Fueled by the development in nanoscience, there has been a surge in activity in EC-SERS since the 1990s. One of the most significant works for preparing SERS substrates in a well-controlled manner was proposed by Natan et al. in 1995.[21] In this work, highly SERS-active monodisperse Au or Ag nanoparticles were assembled on organosilane-polymer-modified solid substrates. Furthermore, conducting materials, such as indium-doped SnO_2 and Pt could be used as the substrate to immobilize the colloids, which provided a new way for applications in spectroelectrochemistry.

An alternative approach to prepare large-area and well-ordered SERS substrates is nanosphere lithography (NSL), which has been predominantly developed by the Van Duyne group[67,79,80] and Bartlett group[81,82] since the early 2000s. In a representative procedure of the NSL method, monodispersed silica or polystyrene (PS) nanospheres are first self-assembled on the surface of a conductive substrate to obtain a monolayer or multilayers of a two-dimensional (2D) colloidal crystal mask, and then it is used as a template for the preparation of SERS-active metal films over nanosphere (MFON) electrodes[80] or periodic particle arrays (e.g., metal nanotriangles).[83]

2.2.3. EC-SEIRAS. In 1980, a few years after the discovery of the SERS effect, Hartstein et al. reported surface-enhanced infrared absorption spectroscopy (SEIRAS), in which the authors claimed that the IR absorption of organic molecular monolayers was enhanced by a thin metal overlayer and underlayer in a ATR geometry.[84] In this work, the silicon plate was first deposited with molecular monolayers of organic acids to prepare the sample. And then, the overlayer and underlayer made of thin films of Ag or Au with a thickness less than 60 Å were evaporated. However, the studied frequency region in the IR experiments was limited to above 2000 cm^{-1} (in particular, the C-H stretching modes near 2900 cm^{-1}) due to the absorption of silicon, which is insufficient for the examination of a new surface enhancement effect considering the possible contamination by hydrocarbons.[85–87]

In 1982, Suëtaka et al. carried out a detailed study of the SEIRAS effect, where the IR absorption enhancement of fingerprint vibration bands below 2000 cm^{-1} from p-nitrobenzoic acid (e.g., NO_2 symmetric stretching at 1345 cm^{-1}) was examined.[85] They found that the absorption enhancement on a ~5 nm thick Ag film evaporated onto a Ge prism was about an order of magnitude.[85] In this work, a thin Ag film with an island structure is necessary for the absorption enhancement, and the Ag thickness plays a dominating role in the enhancement mechanism.[85,86]

Osawa et al.[22,87–90] and Suëtaka et al.[85,86] delved deeply into the mechanism of SEIRAS in the 1980s to 1990s. It is worth noting that SEIRAS did not receive much attention due to limited enhancement in 1980s, and since the 1990s, it has received renewed interest owing to its applications,[87] and in particular, many efforts have been devoted to the preparation and characterization of SEIRAS-related nanoparticles or nanostructures.[61,91,92] Nowadays, the SEIRAS effect is applicable to a variety of surface adsorbed species on various metal films, such as Ag, Au, Cu, Pt, Pd, In, Ni, Al, etc.[52,61,93]

After the pioneering work, SEIRAS has been developed to promote the application of IR spectroscopy to the electrochemical interface, leading to a notable growth of EC-SEIRAS studies since the mid-1990s.[22–25,87] Significantly, along with the SEIRAS effect, the application of the ATR mode greatly facilitates the EC-IR measurement on the metal film electrodes, and the Osawa group pioneered the ATR-SEIRAS studies of molecular adsorption and reactions at the electrode–electrolyte interface in the 1990s (a representative ATR-cell is shown in Fig. 6A).[23–25,61,87] To realize high-performance electrochemical ATR-SEIRAS, it is crucial to prepare suitable thin metal films on the optical window. Advanced by nanotechnology, the ATR-SEIRAS mode has been revived due to the development of fabrication techniques with which different kinds of metal materials, such as Ag, Au, Cu, Pt, Pd, In, Ni, and Al,[52,61,93] can be more easily deposited in the form of thin films on window materials through which IR light propagates.
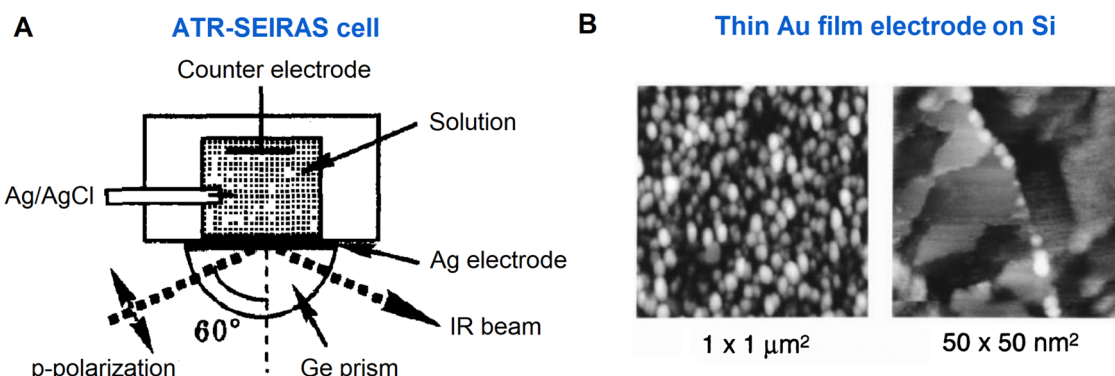

Fig. 6 (A) Schematic of an ATR-SEIRAS cell. (B) STM images of a thin Au(111) film electrode for EC-SEIRAS experiments, where the electrode was obtained by vacuum-evaporation on a Si prism. Fig. 6A is reproduced with permission from ref. 22. Copyright 1993 Elsevier B.V. Fig. 6B is reproduced with permission from ref. 25. Copyright 1998 American Chemical Society.

Interestingly, as shown in Fig. 6B, vacuum evaporated gold films with ordered nano-island structures can provide suitable SEIRAS enhancement while still exhibiting the electrochemical response of Au(111) single crystal electrodes.[23–25]

In addition to the SEIRAS effect, the presence of thin metal films introduced another interesting phenomenon at the electrochemical interface. An abnormal infrared effect (AIRE) was observed in the IR study of molecules adsorbed on the electrode surface in the presence of metal films, primarily by Sun *et al.*[94,95] in the late 1990s. The IR spectra of CO and SCN^- adsorbed on thin Pt, Pd, and Rh films deposited on glassy carbon (GC) electrodes showed an inversion in the sign of IR bands as well as an IR absorption enhancement. The AIRE was directly related to the reflection of IR light from the metal thin film electrode; however, it was not limited to the SPR-active coinage metals (*i.e.*, Au, Ag, and Cu) and was not sensitive to surface roughness, which is not similar to the SEIRAS effect.[94,95]

2.2.4. EC-SESFG. It is important to note that, due to the SPR effects, the surface-enhanced SFG (SESFG) experiments have been conducted on the surfaces of thin metal films[96,97] or nanoparticle substrates.[98–100] For instance, the nanoparticles coupled with a Au film can provide a 10^5-fold enhancement in SFG signals of surface adsorbed *p*-mercaptobenzonitrile.[100] As a nonlinear spectroscopy method, the configuration of the electrochemical cell and optic system in the electrochemical SFG measurement is demanding; therefore, SESFG offers a new opportunity for ultra-sensitive nonlinear coherent spectroscopy at electrochemical interfaces, *e.g.*, theoretically, the enhancement of IR absorption can compensate for the attenuation of IR light in the electrolyte, facilitating the EC-SFG measurement while avoiding the complications of using a thin-layer cell. However, because SFG requires high smoothness of the substrate surface, and due to the intrinsic high surface sensitivity and selectivity, normal mode SFG is preferred for spectroelectrochemical studies.[56]

Based on the surface enhancement effect, the vibrational spectroscopic signal of surface-adsorbed molecules can be enhanced up to several orders of magnitude (*e.g.*, a Raman signal enhancement greater than 10^6-fold in EC-SERS), enabling the *in situ* vibrational detection of a (sub)monolayer of molecules on the surface.[45,50] Thanks to the pioneering work and the excellent surface detection sensitivity, electrochemical surface-enhanced spectroscopy has become a significant experimental subfield in spectroelectrochemistry.[5,45,61,101,102]

2.3. Phase III

In spectroelectrochemistry, the use of structurally well-defined electrode surfaces, such as an atomically flat single-crystal electrode surface, can help to determine the coverage, arrangement, and orientation of adsorbed molecules, as well as the electrode surface state and optic field, respectively. Therefore, the substrates with well-defined surfaces greatly facilitate the systematic research studies on the electrochemical mechanism and its correlation with theory. In phase III of the development of electrochemical optical spectroscopy, as advanced by the rapid development of nanoscience since the 1990s, considerable efforts had been devoted to the realization of spectroelectrochemical measurements on well-defined surfaces.

2.3.1. Electrochemical vibrational spectroscopy on well-defined surfaces. The external-reflection spectroscopic configuration (Fig. 4A) further promoted the *in situ* measurement of IR and SFG spectroscopy on structurally well-defined electrodes, in particular, the single-crystal electrode surfaces.[26–28,31,32,103,104] From the late 1980s to the early 1990s, pioneering experiments using IR or SFG spectroscopy to elucidate the electrochemical properties of surface adsorbed species (such as carbon monoxide,[26,27] hydrogen,[28,31] cyanide,[32] *etc.*) on the surface of noble metal single crystal electrodes paved a new way for understanding the relationship between the surface structure and electrochemical process by means of vibrational spectroscopy.

However, as compared to IR and SFG spectroscopy, Raman spectroscopic measurement on well-defined surfaces is more challenging due to the intrinsically extremely low optical cross-section. As shown in Fig. 4B, although the SERS effect greatly enhances the Raman signal of surface-adsorbed species, the electrode surface needs to be roughened or nanostructured to excite the localized surface plasmon resonance (LSPR) for high SERS activity.[50] As a result, the Raman signal responses are inhomogeneously distributed over the electrode surface with ill-defined morphology. Furthermore, spatially-resolved SERS measurements on nanostructured electrode surfaces revealed that the plasmonic "hotspots" with large electromagnetic field enhancement can even provide site-specific redox potentials.[105] Therefore, spectroelectrochemical studies on atomically flat single-crystal surfaces are important in surface electrochemistry, but highly challenging for conventional SERS. This intrinsic difficulty has led to a gradual decrease in the tidal wave of SERS research since the late 1980s.[106] Different from the nanostructure-based SERS, an alternative way to enable the SERS effect on a smooth metal surface is to excite the surface plasmon polariton (SPP) through an ATR configuration (Fig. 4C), including the Otto configuration and Kretschmann configuration.[60] In 1991, based on a Kretschmann configuration, the EC-Raman measurement was conducted on a well-defined Ag(111) film electrode epitaxially grown on mica.[29] On the other hand, with an ATR-Otto configuration, the facet-dependent adsorption of pyridine was studied on three low-index Cu single-crystal electrode surfaces, *i.e.*, Cu(111), (100), and (110), respectively.[30] But there are still several limitations: first, the signal is still very weak, and a few systems with very strong Raman signals, *e.g.*, *para*-nitrosodimethylaniline[29] and pyridine,[30] can be studied; second, related optical system configurations and electrochemical cells are complicated.

2.3.2. EC-SHINERS. In 2010, to solve the problems of material and surface morphology generalities in conventional SERS, Tian *et al.* invented a new Raman spectroscopic mode by isolating the highly SERS-active Au nanoparticle core with an ultra-thin and pinhole-free dielectric SiO_2 (or Al_2O_3) shell, which was named shell-isolated nanoparticle-enhanced Raman spectroscopy (SHINERS).[33] Fig. 7A–C show the comparison between the working principles of conventional SERS using

3588 | *Chem. Soc. Rev.*, 2024, **53**, 3579–3605

This journal is © The Royal Society of Chemistry 2024
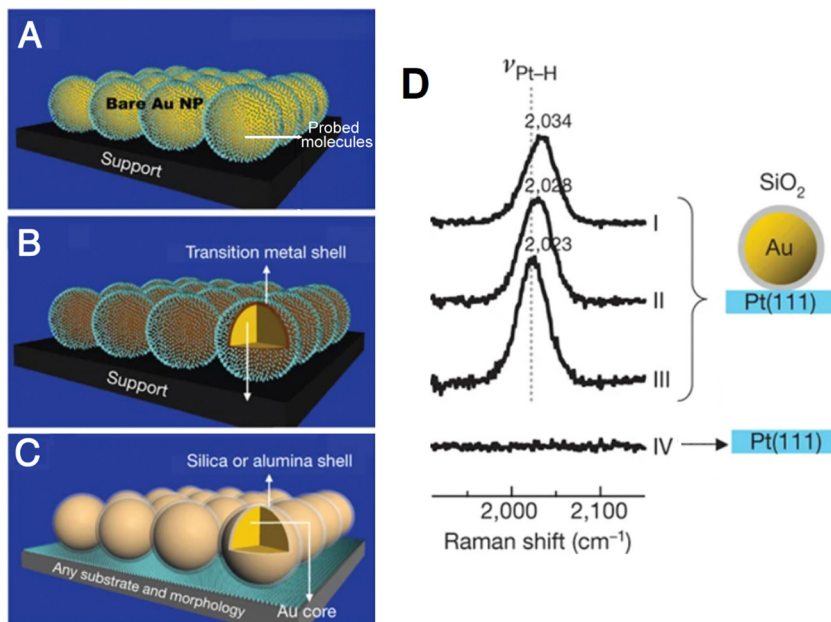
Fig. 7 (A) and (B) Schematic of conventional SERS using Au nanoparticles (A) and transition metal shell coated Au nanoparticles (B). (C) Schematic of SHINERS. (D) Potential-dependent SHINERS spectra of hydrogen adsorbed on Pt(111) electrode surfaces. Reproduced with permission from ref. 33. Copyright 2010 Macmillan Publishers Limited.

bare Au nanoparticles (Fig. 7A) and Au core–TM shell nanoparticles (Fig. 7B), and the SHINERS method (Fig. 7C). Because the shell of shell-isolated nanoparticles (SHINs) is chemically and electrically inert, the SHINERS method can prevent the interference due to the contact of the analyte and electrolyte with the Au core, while allowing the SERS enhancement generated by the SERS-active Au core to penetrate through the shell, thereby offering largely enhanced Raman signals from the electrode surface species. As shown in Fig. 7D, the important potential-dependent adsorption of hydrogen on the Pt(111) electrode is revealed by SHINERS spectra (curves I to III), which cannot be obtained on a bare single-crystal electrode through normal Raman spectroscopy (curve IV). Hence, the SHINERS method is suitable for the spectroelectrochemical study on weakly SERS-active or SERS-

inactive material surfaces, such as the important single-crystal electrode surfaces.

2.3.3. Tip-based electrochemical vibrational spectroscopic modes. Meanwhile, the development in the field of scanning probe microscopy (SPM), including scanning tunneling microscopy (STM) and atomic force microscopy (AFM), has provided an unprecedented high spatial resolution for probing structurally well-defined surfaces in an electrochemical environment,[107–109] and has further inspired the idea of tip-based electrochemical vibrational spectroscopy (Fig. 4D). In 1994, Tian *et al.* conducted a pioneering study by combining STM and Raman spectroscopy to *in situ* measure the surface morphology and vibrational signal from the electrode simultaneously (the schematic of the combined base for simultaneous STM and Raman spectroscopy is presented in Fig. 8A).[110,111]
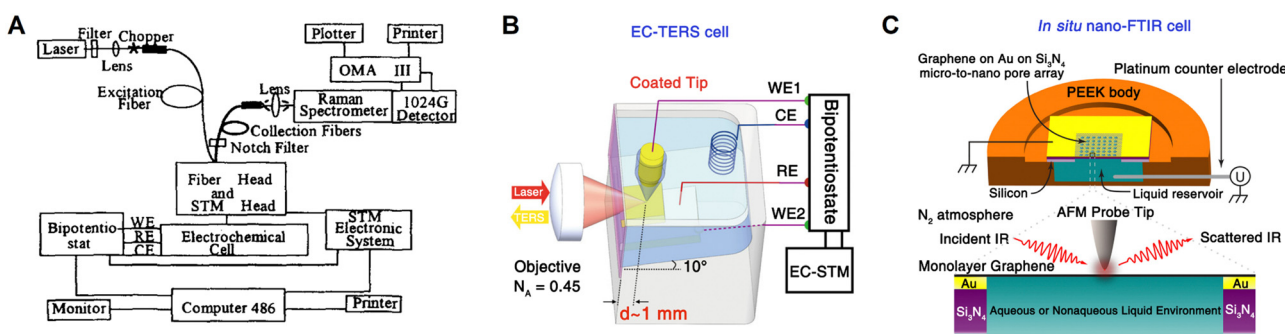
Fig. 8 Schematics of the combined base of simultaneous STM and Raman spectroscopy (A), *in situ* cell of EC–TERS (B) and nano–FTIR (C), respectively. (A) is reproduced with permission from ref. 110. Copyright 1996 Elsevier. (B) is reproduced with permission from ref. 34. Copyright 2015 American Chemical Society. (C) is reproduced with permission from ref. 36. Copyright 2019 American Chemical Society.

This journal is © The Royal Society of Chemistry 2024

Chem. Soc. Rev., 2024, **53**, 3579–3605 | 3589

Based on SPM, tip-enhanced Raman spectroscopy (TERS) was independently invented by several groups in 2000,[112–115] which can provide a Raman spectroscopic imaging resolution at a nanometer-scale.[106] However, it is highly difficult to combine TERS and electrochemistry in the limited space of a SPM system. In 2015, Ren et al.[34] and Van Duyne et al.[35] independently reported electrochemical TERS (EC-TERS), ushering in a new era of nanospectroscopic research at electrochemical interfaces. On a Au(111) single-crystal surface, EC-TERS can reveal the potential-dependent protonation and deprotonation of the adsorbed aromatic molecules (a typical cell for EC-TERS is shown in Fig. 8B),[34] and with the further improvement in sensitivity, this technique is currently able to probe a chemical reaction in solution with a spatial resolution of around 5 nm.[116]

On the other hand, the combination of SEIRAS effect and scanning near-field optical microscope has advanced nanoscale IR spectroscopy on a well-defined surface.[117] In 2019, based on AFM, the first in situ electrochemical Fourier transform infrared nanospectroscopy (nano-FTIR, Fig. 8C) was realized on a graphene electrode surface, where the potential-dependent behavior of SO_4^{2-} and NH_4^+ ions at the graphene/electrolyte interface was studied using nano-FTIR spectra.[36] Furthermore, the combination of nano-FTIR and ATR-FTIR methods allows for the probing of subsurface depths at the nanoscale and microscale, respectively. This was achieved by applying a custom-built solid polymer electrolyte cell with a single layer of graphene as the working electrode, which is IR transparent.[118] As a result, it was capable of simultaneously in situ studying both the electrochemical interface together with the bulk phase of solid polymer electrolyte.

Furthermore, scanning electrochemical microscopy (SECM) is a unique method to investigate the nanoscale information of structure–activity on electrode surfaces, in which an ultramicroelectrode (UME) tip is positioned near the substrate surface, which drives a redox reaction that records the diffusion-limited currents generated during scanning of the substrate surface, thus offering information on the surface morphology and local interfacial electrochemical activity.[119] Combining SECM with optical spectroscopy enables the simultaneous in situ studies of the electrochemical processes and molecular vibrational signatures in local regions,[120,121] i.e., to study local surface modifications with self-assembled monolayers[122] and the surface pH perturbations induced by the UME tip-driven hydrogen evolution reaction (HER).[123]

2.4. Phase IV

2.4.1. *Operando* methodology. After entering the 21st century, in order to understand the electrochemical structure and process in an electrochemical device under the real working conditions, the enthusiasm of electrochemical researchers to perform *operando* spectroelectrochemistry is ever growing. Therefore, in phase IV, the latest phase in the development of electrochemical vibrational spectroscopy, we will focus on the advances of *operando* spectroelectrochemistry methodology.

Unlike the concepts of *ex situ* and *in situ*, which were proposed in early times and have been applied ever since, the term *operando* originates from the Latin gerund, and it was introduced in 2002 as a tentative name for "real" reaction *in situ* spectroscopy.[124] Both the terms *in situ* and *operando* originated from heterogeneous catalysis research,[125] while the *operando* methodology was first used for the combination of *in situ* spectroscopy characterization and simultaneous evaluation of both the structure and activity of catalysts under working conditions.[124,126] Figuratively speaking, *ex situ* techniques study a dead fish out of water (or a sliced fish), *in situ* techniques study a live fish restricted to a small fishbowl, while *operando* techniques can comprehensively study a fish swimming freely in the ocean. In contrast to *ex situ* techniques normally examining the sample outside the electrochemical working environment, *in situ* and *operando* techniques can study the surface and phase changes in the electrode bulk, and the electrochemically generated reaction intermediate. Normally, *in situ* measurements are suitable for the fundamental study on a well-defined or model electrode surface, whereas *operando* characterization emphasizes on the measurements in a practical/commercial device or an architecture highly resembling the practical one.[101,127–129]

2.4.2. *Operando* electrochemical vibrational spectroscopy. The pioneering *operando* EC-IR and EC-Raman studies were conducted in the early 2010s.[37–39] Nowadays, as the emerging electrochemical interfaces become more complicate, considerable efforts are devoted to designing a suitable cell for *operando* measurement (especially, the studies of batteries under real working conditions).[101,127–129] Recently, to monitor the dynamic chemical information in a full battery under real working conditions, the *operando* spectroscopic methods that combine fiber probes and vibrational spectroscopy have been developed.[40,41,130,131] In the meantime, artificial intelligence (AI) has emerged as a promising approach to revolutionize the research paradigm of chemistry and material science, and is thus expected to offer more advances in the data-driven *operando* spectroelectrochemical techniques.[132] The novel fiber-based electrochemical vibrational spectroscopic mode (Fig. 4E) will be discussed in Section 4.2.2.

3. Advances in *in situ* and *operando* applications

Nowadays, with a growing impact on electrochemical fields as diverse as electrochemical energy storage and conversion, electrolysis, electroplating, corrosion, electrochemical synthesis, biological electron-transfer processes, etc., *in situ* or *operando* characterization methods with desirable detection sensitivity and resolutions to understand the structure and dynamics of electrode–electrolyte interfaces/interphases have become increasingly significant.[5,52,61,101] In the following, we will focus on the recent advances in *in situ* and *operando* applications of electrochemical vibrational spectroscopy.

3590 | *Chem. Soc. Rev.*, 2024, **53**, 3579–3605

This journal is © The Royal Society of Chemistry 2024

3.1 Electrical double layer

Probing the composition and structure of the electrical double layer is highly significant in electrochemical studies. Interfacial water has an important impact on the physical and chemical properties of the electrical double layer, and the EC-Raman investigation of interfacial water was first carried out by Fleischmann *et al.* in 1981.[133] However, the conventional Raman spectroscopy is incapable of probing interfacial water on single-crystal electrodes with atomically flat surfaces, which limits the understanding of the atomic structure of interfacial water. As a key figure of merit, SHINs can be used as Raman signal amplifiers to obtain vibrational spectra on the surface of single-crystal electrodes without interference from the bulk electrolyte (Fig. 9A–C show the working principle and surface Raman signal enhancement in SHINERS during the study of interfacial water[134]).

As shown in Fig. 9D and E, the SHINERS method is suitable for the *in situ* probing of the adsorption of interfacial water on Au(111)[134,136] and Pd(111)[135] electrodes, respectively. SHINERS spectra of interfacial water, particularly the OH stretching modes in the spectral range from 3000 to 3800 cm^{-1}, show distinct potential dependence on both Au(111) (Fig. 9D) and Pd(111) (Fig. 9E) electrodes, indicating the changes in the structure of interfacial water, *i.e.*, the orientation of interfacial water and related hydrogen-bonding networks. On the Au(111)

electrode, the Stark tuning rate can be derived from the Raman frequency shift of the interfacial water under bias conditions, with which it is capable of revealing two structural transitions of interfacial water, *i.e.*, from a "parallel" structure to a "one H-down" structure and then to a "two-H-down" structure, as the electrode potential was negatively scanned from potential of zero charge (PZC) toward the hydrogen evolution reaction (HER) region.[134] On the surface of the Pd(111) electrode, the interpretations on the OH stretching mode indicate that interfacial water consists of hydrated cations and hydrogen-bonded water. Meanwhile, the interfacial water structurally transformed from a randomly distributed state to an ordered one in the HER region owing to the cation cooperation and the potential changes.[135]

Vibrational IR-visible SFG spectroscopy is a unique spectroscopic method for studying water molecules at the interface, where the OH frequency and intensity reveal the hydrogen bonding strength and ordering of water molecules,[137] enabling the sensitive nonlinear spectroelectrochemical study of the structures of interfacial water and the electrode double layer.[14,53,102,138–142] As shown in Fig. 10A and B, Benderskii *et al.* investigated the IR-visible SFG signal of D$_2$O on a monolayer graphene electrode surface, and they found a pronounced asymmetry in the response of OD stretching to the positive and negative potentials.[140] To detect the charge-neutral
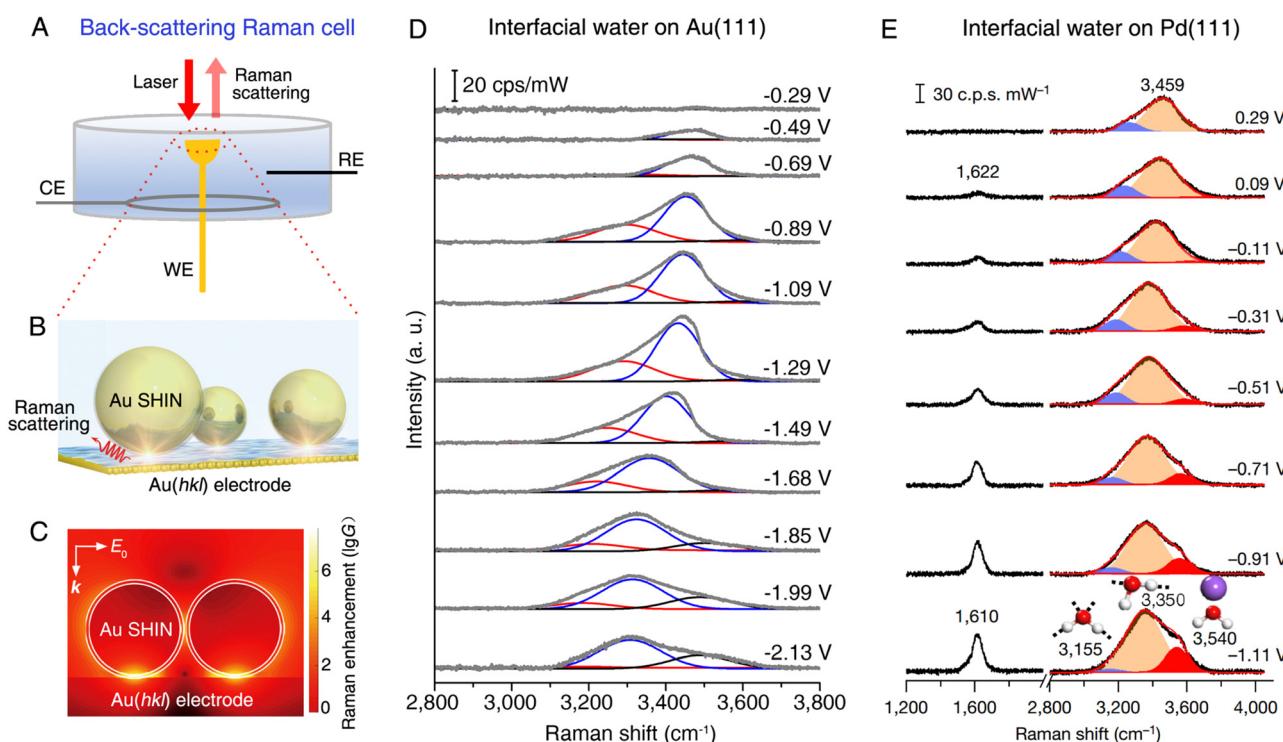
Fig. 9 (A) Schematic of a back-scattering Raman cell for the SHINERS method on a single-crystal electrode. (B) Schematic of EC-SHINERS for interfacial water measurement. (C) Finite-element-method simulation of Raman signal enhancement on a Au electrode surface in EC-SHINERS. (D) *In situ* EC-SHINERS spectra of interfacial water on the Au(111) electrode in a 0.1 M Na$_2$SO$_4$ solution. The potential is referenced to potential of zero charge. (E) *In situ* EC-SHINERS spectra of interfacial water on the Pd(111) electrode in a 0.1 M NaClO$_4$ solution (pH 11). The Pd(111) electrode is obtained by coating a Pd monolayer onto a Au(111) electrode surface and the potential is referenced to a reversible hydrogen electrode. (B)–(D) reproduced with permission from ref. 134. Copyright 2019 Springer Nature. (E), Reproduced with permission from ref. 135. Copyright 2021 Springer Nature.

This journal is © The Royal Society of Chemistry 2024

Chem. Soc. Rev., 2024, **53**, 3579–3605 | **3591**
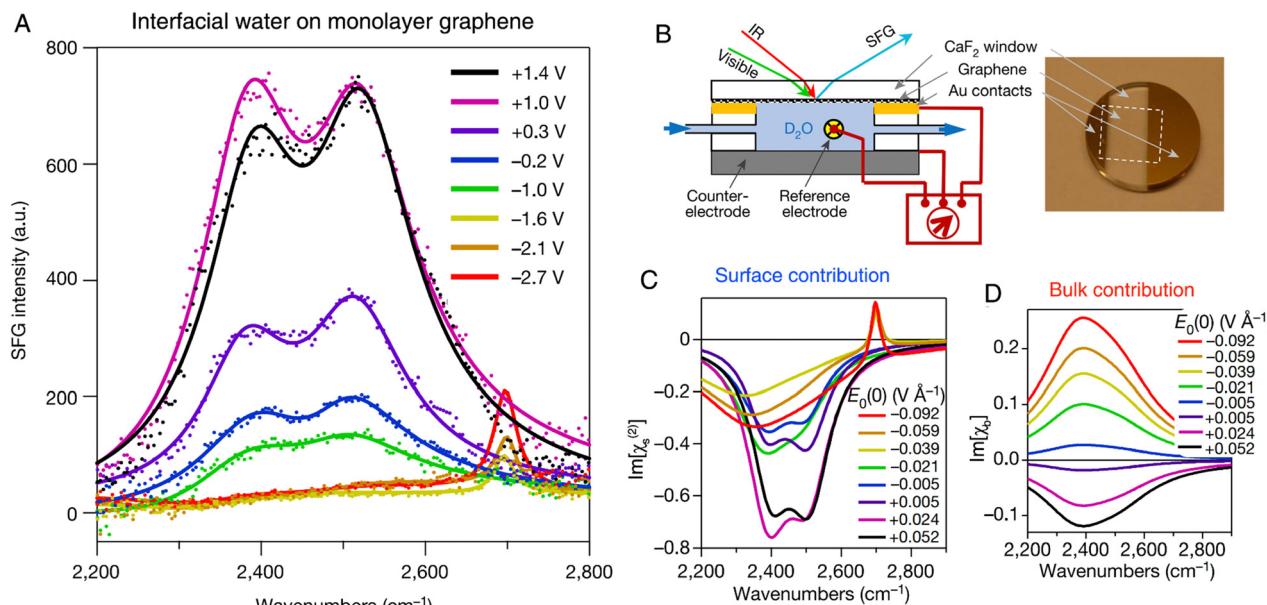
Fig. 10 (A) *In situ* SFG spectra of D_2O at the graphene electrode (no electrolyte is added to D_2O). The potential is referenced to a Ag/AgCl electrode. (B) Schematic of an electrochemical cell and the corresponding photograph of a graphene electrode for SFG experiments. (C) and (D) The extracted surface (C) and bulk (D) contribution from SFG spectra as a function of the applied field. Reproduced with permission from ref. 140. Copyright 2021 Springer Nature.

point on the graphene electrode, the minimum of potential-dependent G-band Raman frequency of graphene was measured and it was found at $\sim$ +0.1 V (*vs.* Ag/AgCl). For the spectra obtained at potentials more negative than −1.6 V, only a relatively narrow peak at 2697 cm^{-1} was found, which was assigned to the free OD stretching mode of D_2O in the topmost monolayer (Fig. 10A). However, when the potential was set to positive values above −1.0 V, only the characteristic broad hydrogen-bonded bands from $\sim$2300 to $\sim$2700 cm^{-1} were observed and the narrow free-OD band disappeared.

SFG is nominally a second-order nonlinear process (the second-order susceptibility tensor of the medium can be expressed as $\chi^{(2)}$), but the static electric field at the charged graphene–D_2O interface gave rise to a third-order contribution (*i.e.*, the $\chi^{(3)}$ term). In contrast to the $\chi^{(2)}$ term, which originates from only a few monolayers of water on surface, the $\chi^{(3)}$ term may contain the contribution from the region through which the static electric field penetrates, *i.e.*, the Debye screening length (in the order of 1 μm in this work). By comparing the imaginary parts of the surface (Im[$\chi^{(2)}$], Fig. 10C) and bulk (Im[χ_b], Fig. 10D) contributions from the spectra, the extracted potential-dependent Im[$\chi^{(2)}$] does not follow the linear response as that of Im[χ_b], exhibiting significant asymmetry at positive and negative potentials. The unusual nonlinear response of interfacial water to the applied electric field suggested that treating interfacial water as a simple linear dielectric medium should be carefully considered and further examined.

3.2. Electrocatalysis

Vibrational spectroscopy (such as IR and Raman spectroscopy) exhibits an energy resolution of around two orders of magnitudes higher than conventional electrochemical techniques; therefore, it can be used to carefully study the molecular structure of adsorbed molecules or oxidation (reduction) of molecules, enabling a detailed analysis of the reaction mechanism in electrocatalysis. For instance, in the spectroelectrochemical study of electrocatalytic reactions, IR absorption spectroscopy has been combined with cyclic voltammetry (CV) in the *in situ* investigation of direct oxidation of methanol on the Pt electrode.[143] In the CVs of both the positive and negative potential sweeps of the polycrystalline Pt electrode, the dominant and shoulder peaks were almost merged. However, in the corresponding IR absorption spectra with a spectral resolution at 4 cm^{-1}, the linearly and bridged-bonded CO molecules were clearly differentiated at the beginning of potential scan. It was clearly demonstrated that vibrational spectroscopy is beneficial for a higher energy resolution to identify the adsorbed species as compared to the conventional electrochemical technique.[143] With this intrinsic advantage, IR spectroscopy has received great attention in the study of significant electrochemical CO_2 reduction reactions (CO$_2$RR), *i.e.*, the CO$_2$RR on Cu electrocatalysts, where Cu is one excellent electrocatalyst material for CO2RR and also a suitable substrate for high SEIRAS activity.[61,144] Based on *in situ* ATR-SEIRAS, Shao *et al.* studied the role of a bicarbonate-based electrolyte, a widely used aqueous electrolyte, in the CO$_2$RR on a Cu thin film electrode supported on a Au substrate.[145] As the potential was scanned from +0.3 toward −1.3 V in CO$_2$-saturated $KHCO_3$, they observed several distinct vibrational features in the spectral region from 1300 to 2400 cm^{-1}, where the depletion of CO_2 (*i.e.*, the IR absorption band at $\sim$2340 cm^{-1}) and increase of adsorbed CO (*i.e.*, the broad band at $\sim$2080 cm^{-1}) become

3592 | *Chem. Soc. Rev.*, 2024, **53**, 3579–3605

This journal is © The Royal Society of Chemistry 2024
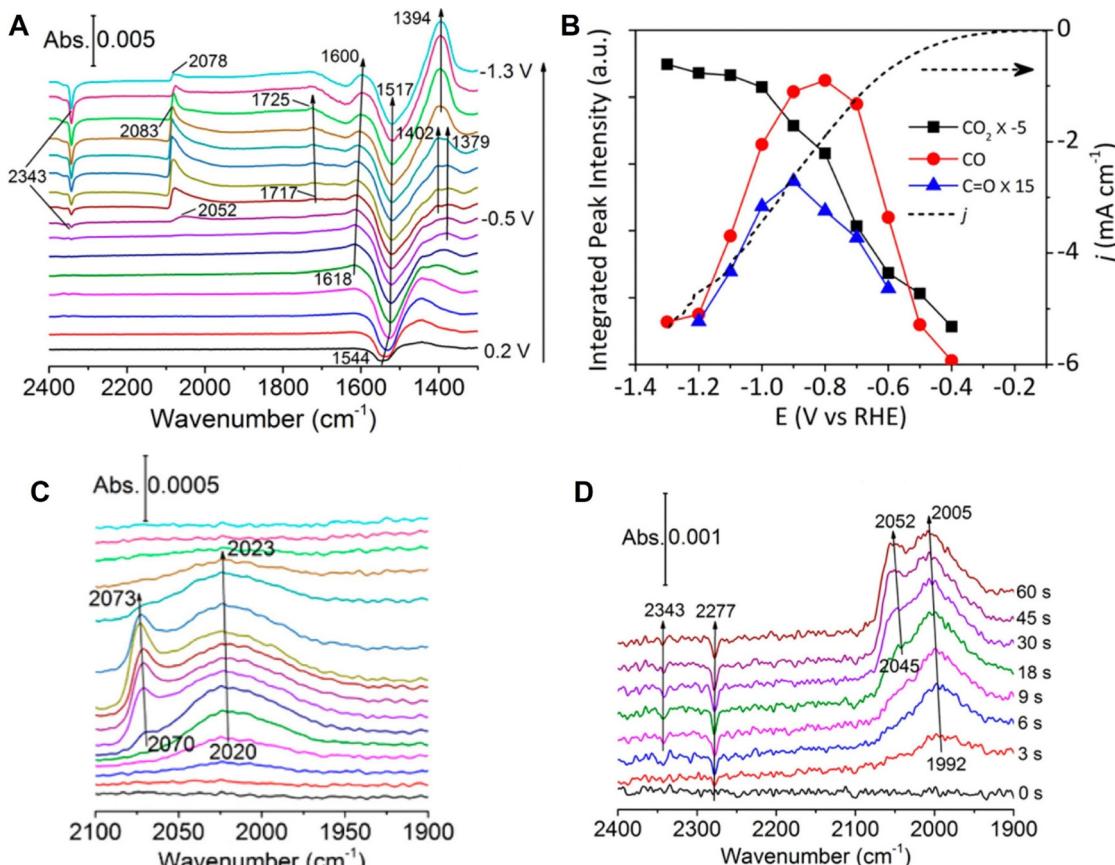
Fig. 11 (A) *In situ* ATR-SEIRAS spectra on a Cu thin film electrode in a CO$_2$-saturated 0.1 MKHCO$_3$ electrolyte. (B) Corresponding cyclic voltammogram curve (dotted line) and peak intensities in (A). (C) ATR-SEIRAS spectra measured in an Ar-saturated 0.1 MKHCO$_3$ electrolyte. (D) Time-dependent ATR-SEIRAS on the Cu thin film electrode after stepping from 0.2 to −0.6 V *vs.* RHE in a CO$_2$ purged 0.1 M KH^{13}CO$_3$ electrolyte. In (A) and (C), spectrum obtained at 0.3 V was used as a reference. In (D), the reference spectrum was obtained at 0.2 V. Reproduced with permission from ref. 145. Copyright 2017 American Chemical Society.

visible at $\sim$ −0.4 V *vs.* RHE, close to the onset of the reduction current in the linear scanning voltammogram at $\sim$−0.3 V (Fig. 11A and B). However, they found that the surface-adsorbed CO species could be detected in the absence of CO$_2$ purge, *i.e.*, the bands around 2020 and 2070 cm^{-1} originating from the different adsorption configuration of CO on Cu were still observable in the control experiment in Ar-saturated 0.1 M KHCO$_3$ (Fig. 11C). This observation indicated that bicarbonate anions were the main CO$_2$ source in the CO$_2$RR process on the Cu electrode. Furthermore, they carried out an isotopic experiment by purging the unlabeled CO$_2$ to a labeled KH^{13}CO$_3$ electrolyte and measured the time-dependent SEIRAS spectra at −0.6 V. As shown in Fig. 11D, a depletion of ^{13}CO$_2$ in the solution was observed at 2277 cm^{-1} in the first 3s, followed by the simultaneous appearance of adsorbed ^{13}CO at $\sim$1990 cm^{-1}, which offered direct spectroscopic evidence that the CO$_2$ in equilibrium with CO$_3^-$ was the main CO$_2$ source.[145]

The understanding of the relationships between the surface structure and catalytic activity can greatly benefit the design and synthesis of high-performance electrocatalysts. Pt electrocatalysts play a significant role in the oxygen reduction reaction (ORR); however, the related Raman spectroscopic studies are limited to nanostructured Pt electrode surfaces; therefore they are unable to investigate the structure–activity relationships on structurally well-defined single-crystal electrodes.[71] To unravel the reaction mechanism of ORR on a single-crystal Pt(*hkl*) electrode surface, Li *et al.* used *in situ* EC-SHINERS to identify the intermediates involved in the ORR in both acidic environments, in which they found different pathway mechanisms of the ORR process on Pt(111), Pt(100), and Pt(110) electrode surfaces.[146] As shown in Fig. 12, they spread SHINs (pinhole-free Au@SiO$_2$ nanoparticles) onto the Pt single-crystal electrode surface to enhance the Raman signal from the interfacial region (the related experimental configuration is similar to that illustrated in Fig. 9). In a 0.1 M HClO$_4$ solution, *in situ* EC-SHINERS spectra were recorded on the Pt(111) electrode from 1.1 to 0.5 V *vs.* RHE, in which a Raman peak of 732 cm^{-1} appeared at 0.8 V (Fig. 12A). Based on the deuterium isotopic substitution experiment and density functional theory (DFT) calculations, this peak was assigned to the O–O stretching mode of HO$_2$* species on Pt(111). In addition, as revealed in Fig. 12B, the Raman peak corresponding to HO$_2$* species appeared at a potential very close to the potential at which the ORR process achieved the limiting diffusion current

This journal is © The Royal Society of Chemistry 2024

Chem. Soc. Rev., 2024, **53**, 3579–3605 | **3593**
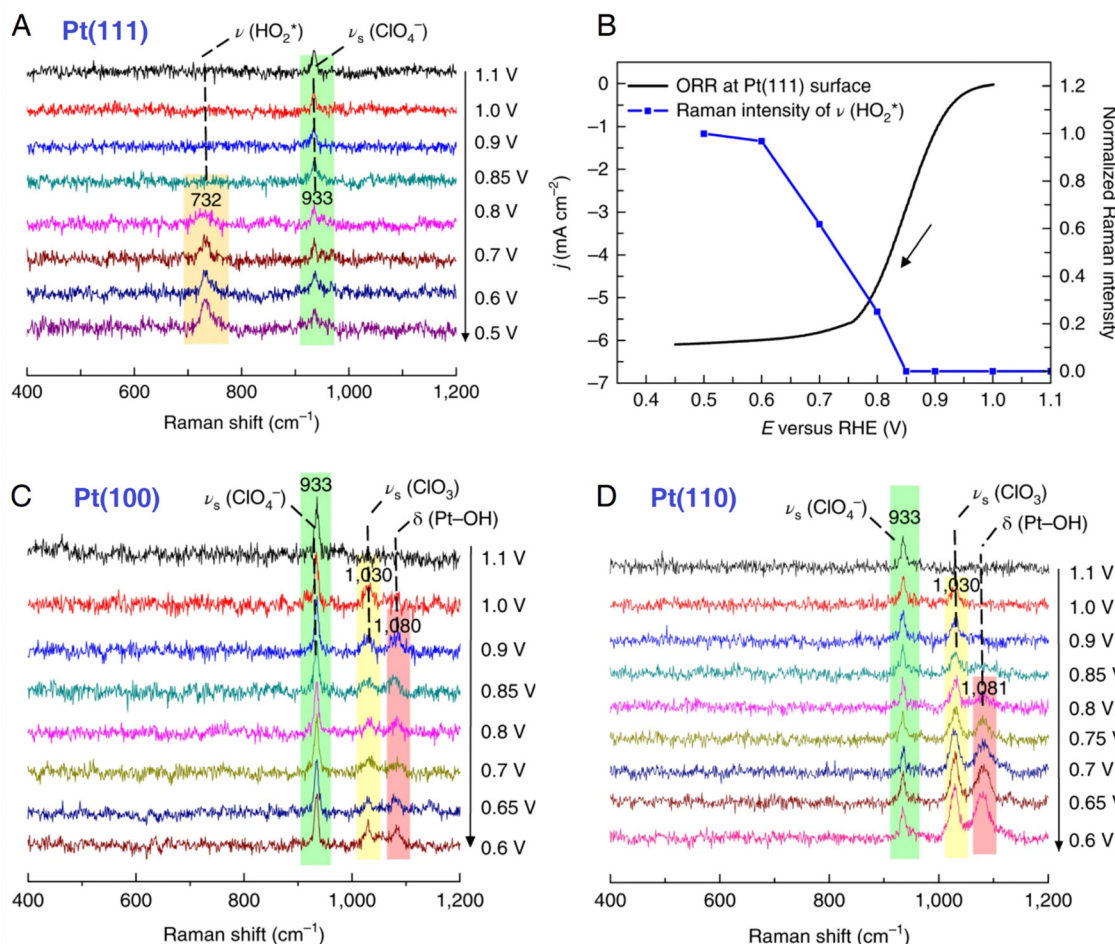
Fig. 12 (A) *In situ* EC-SHINERS spectra on the Pt(111) electrode in O_2-saturated 0.1 M $HClO_4$. (B) Potential-dependent Raman intensity of HO_2^* species on Pt(111) *versus* ORR current. ORR current was obtained in a O_2-saturated 0.1 M $HClO_4$ solution using a rotating disk electrode Pt(111) electrode with a rotation rate of 1600 rpm. and a scan rate of 50 mV s^{-1}. (C) and (D) *In situ* EC-SHINERS spectra on Pt(100) (C) and Pt(110) (D) electrodes in O_2-saturatred 0.1 M $HClO_4$. Reproduced with permission from ref. 146. Copyright 2018 Springer Nature.

($\sim$0.7 V), indicating a crucial role of HO_2^* species in the ORR under acid conditions. In sharp contrast, the important HO_2^* species was absent on Pt(100) and Pt(110) electrode surfaces; however, two Raman peaks at 1030 and 1080 cm^{-1} were observed, which were attributed to the symmetric stretching mode of ClO_3 in $HClO_4$ and Pt-OH bending mode OH* species. Apparently, the EC-SHINERS method provided direct spectroscopic evidence of the different ORR mechanisms on three Pt(*hkl*) electrodes in an acidic solution, that is, the ORR on the Pt(111) surface by the generation of HO_2^*, while on Pt(100) and Pt(110) electrode surfaces by the formation of OH*.

3.3   Rechargeable batteries

Recently, *operando* characterization methods have received great attention due to their ability to probe the structural, chemical, and mechanical changes in electrochemical energy devices under their real working conditions.[101,127,147,148] In rechargeable batteries, *operando* methods benefit largely from the collaboratively combination of diverse characterization techniques to understand the complex interrelated

phenomena, such as the relationships between structural transformation and chemical reaction and performance of device.[149] As a representative example shown in Fig. 13, Zhou *et al.* carried out an *operando* spectroelectrochemical study of the anionic redox process in Li-ion batteries by correlating vibrational Raman spectroscopy and differential electrochemical mass spectrometry (DEMS).[150] The exploration of oxygen-related anionic redox (peroxo-like $(O_2)^{n-}$ species) activity in Li-ion batteries opens up a new way for boosting the capacity limit of electrode materials and thus has attracted much interest, but it also calls for advanced *operando* characterization techniques to probe the underlying nature of the anionic redox activity.[151,152] Vibrational Raman spectroscopy is a powerful characterization method of probing oxygen-related species at electrochemical interfaces.[146,153-155] As shown in Fig. 13A, a Li-rich Ni/Co-free O3-type $Li_{0.6}[Li_{0.2}Mn_{0.8}]O_2$ was used as the cathode, and assembled into an *operando* Raman cell with Li foil serving as both the reference and counter electrode. During the first and second charge–discharge cycles, a vibrational feature appeared in the region from 795 to 845 cm^{-1} that was
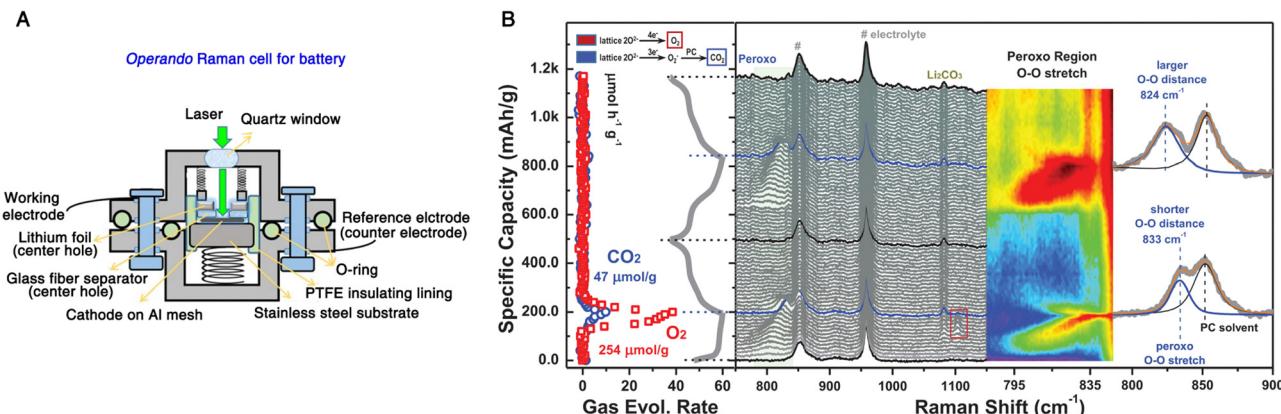
Fig. 13 (A) Schematic of an *operando* Raman cell for Li-ion batteries. (B) *Operando* Raman spectra and DEMS of the gas evolution rate during the first and second cycle of a $Li_{0.6}[Li_{0.2}Mn_{0.8}]O_2$ cathode in an electrolyte consisting of 1 M LiClO$_4$ in propylene carbonate. The peaks marked by the number sign at ~850 and 920 cm^{-1} originate from the electrolyte. Fig. 13A is reproduced with permission from ref. 153. Copyright 2018 the Royal Society of Chemistry. Fig. 13B is reproduced with permission from ref. 150. Copyright 2020 John Wiley and Sons.

attributed to the O–O stretching mode of peroxo species (Fig. 13B), indicating reversible redox properties. However, the peak position shifted toward a higher wavenumber in the second cycle, which suggested a longer O–O distance of peroxo species that would cause the generation of superoxo species (the Raman peak at 1104 cm^{-1} at the end of the first cycle) and gaseous O_2 (a O_2 evolution rate of 254 μmol g^{-1} as quantified by DEMS). Furthermore, the electrochemical decomposition of electrolyte at high voltage and the nucleophilic attack on propylene carbonate by superoxo species could be detected by *operando* Raman spectroscopy, as indicated by the appearance of a Raman peak around 1080 cm^{-1} revealing the formation of Li_2CO_3. Therefore, by combining *operando* Raman spectroscopy and DEMS, relatively reversible oxygen-related redox and electrolyte decomposition processes were monitored in real-time, allowing a better understanding of anionic redox activity in high-capacity electrode materials.

Probing the chemical composition and structures of electrode-electrolyte interfaces (EEIs) or solid-electrolyte interphases (SEIs) is one of the most significant applications of electrochemical vibrational spectroscopy in Li-ion chemistry. Although the thickness of EEIs is only on the nanometer scale, its formation and evolution play a crucial role in achieving a Li-ion battery with high performance and a long cycle life.[156] By coupling with electrochemical operation, optical spectroscopy methods with high surface sensitivity, such as nanostructure- and ATR-based vibrational spectroscopy[56,129] and surface plasmon resonance spectroscopy,[157,158] provide prominent opportunities for *in situ/operando* tracking of the chemical and structural evolution of electrode/electrolyte interfaces or interphases. Shao-Horn *et al.* used *in situ* FTIR spectroscopy to study the formation of EEIs, that is, the oxidation of carbonate-based electrolyte on a Ni-rich $LiNi_{0.8}Co_{0.1}Mn_{0.1}O_2$ (NMC811) electrode surface.[159] Usually, a thin film electrode directly deposited on a prism is preferred for ATR-IR measurements, but it is challenging to prepare a NMC thin film electrode in this configuration. Therefore, in this work, a composite NMC/ glassy fiber was used as a working electrode (positive electrode)

that was placed downward, facing the Pt thin film supported by a CaF$_2$ prism; thereby the reaction intermediates generated from the NMC electrode could be detected through IR absorption in an internal reflection geometry (Fig. 14A). As shown by the *in situ* FTIR difference spectra on an NMC811 electrode charged to 4.4 V in ethylene carbonate with 1.5 M LiPF$_6$ (Fig. 14B), several bands appeared in the spectral region from ~1750 to 1830 cm^{-1} (C=O stretching region) at 3.8 V. These peaks were assigned to vinylene carbonate (~1830 cm^{-1}), ethylene carbonate (~1800 cm^{-1}), Li$^+$-associated ethylene carbonate (~1770 cm^{-1}), and oligomers with ethylene carbonate-like rings (~1760 cm^{-1}), respectively. It is noted that vinylene carbonate is one of decomposed products of ethylene carbonate, that is, vinylene carbonate results from the removal of two hydrogens from ethylene carbonate, forming a C=C bond in the ring. Meanwhile, the oligomer possibly resulted from the opening and polymerization of ethylene carbonate. By potentiostatically holding at 4.4 V for a period of time (0 to 60 min), no obvious changes in the peak intensities were observed (Fig. 14C). In contrast, in the time-dependent measurement at open circuit potential (OCP) following the holding experiment at 4.4 V, the peak intensities of ethylene carbonate, vinylene carbonate, and oligomers decreased quickly, indicating these species diffused away from the EEI at OCP (Fig. 14D). However, a deconvoluted peak at 1813 cm^{-1} hardly changed with increasing time, which was assigned to dehydrogenated ethylene carbonate. This observation suggested that dehydrogenated ethylene carbonate adsorbed on the oxide surface of the NMC electrode, possibly on the surface oxygen through a C–O$_{surface}$ bond generated during the dehydrogenation reaction of ethylene carbonate. As NMC811 was galvanostatically charged to 4.4 V, potentiostatically held at 4.4 V, and rested at OCP, the potential-dependent intensity trends of peaks were consistent with the corresponding voltage profile (Fig. 14E), showing that *in situ* FTIR spectroscopy is sufficient in revealing the chemical and structural changes in the EEI, thus giving insights into the strategies to develop stable and high-performance Li-ion batteries.

This journal is © The Royal Society of Chemistry 2024

Chem. Soc. Rev., 2024, **53**, 3579–3605 | 3595
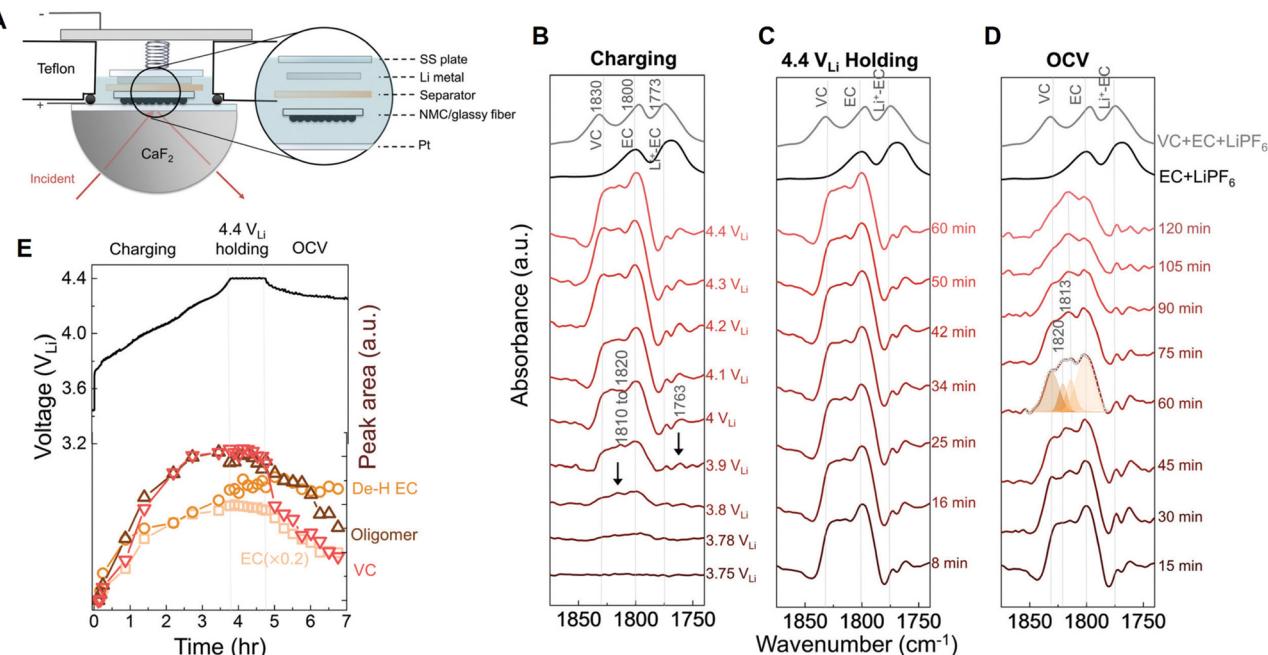
Fig. 14 (A) Schematic of an *in situ* FTIR cell. (B)–(D) *In situ* FTIR difference spectra on the LiNi$_{0.8}$Co$_{0.1}$Mn$_{0.1}$O$_2$ electrode during charging to 4.4 V (B), potentiostatic holding at 4.4 V (C), resting at OCV (D) in ethylene carbonate with 1.5 M LiPF$_6$. (E) Corresponding electrochemical curve of the LiNi$_{0.8}$Co$_{0.1}$Mn$_{0.1}$O$_2$ electrode galvanostatically charged to 4.4 V, held at 4.4 V, and then rested at OCV; and deconvoluted IR intensity of peaks at 1800 cm^{-1} (ethylene carbonate), ~1813 cm^{-1} (dehydrogenated ethylene carbonate, De–H EC), ~1820 cm^{-1} (oligomers), and 1830 cm^{-1} (vinylene carbonate), respectively. OCV is an abbreviation for open circuit voltage, and the potential was referred to Li$^+$/Li. Reproduced with permission from ref. 159. Copyright 2020 the Royal Society of Chemistry.

Solid-state batteries are anticipated to be an alternative to conventional lithium-ion batteries since they replace the flammable liquid electrolyte with a solid electrolyte, allowing for tighter packing of battery components, while also providing safety advantages.[160,161] However, as the active electrode materials are normally opaque, the light beam is unable to penetrate
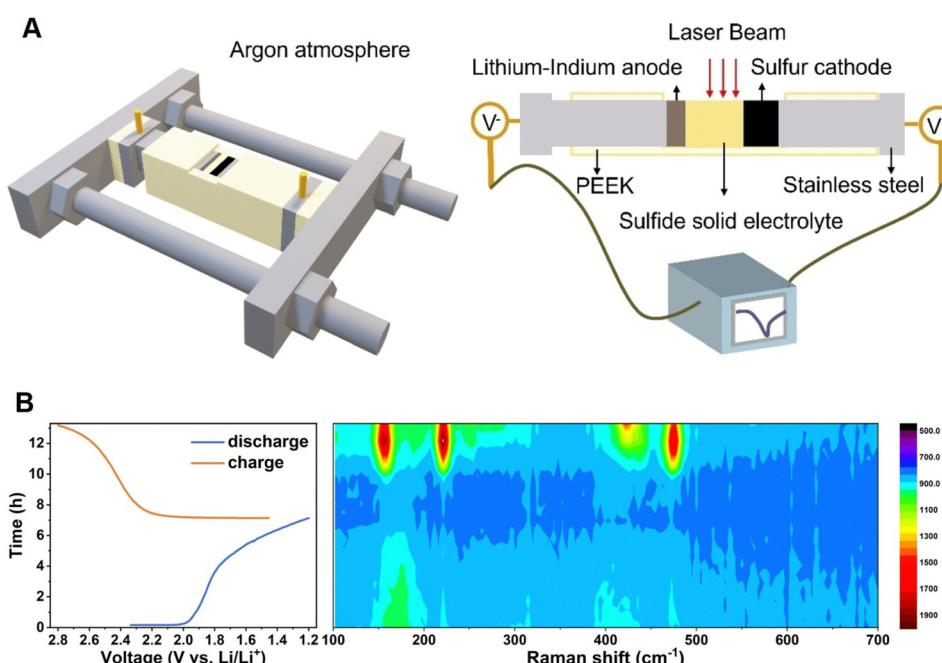
Fig. 15 (A) Schematic of an *operando* Raman spectroscopic cell for solid-state batteries and the corresponding components of the setup. (B) Time–voltage profile of a solid-state Li–S battery and the corresponding *operando* Raman spectra contour. Reproduced with permission from ref. 162. Copyright 2023 Wiley-VCH GmbH.

3596 | *Chem. Soc. Rev.*, 2024, **53**, 3579–3605

This journal is © The Royal Society of Chemistry 2024

Table 2 Comparisons of electrochemical IR, SFG, and Raman spectroscopy

Vibrational spectroscopy	IR	SFG	Raman
Spectroscopic mode	Normal mode; Nanostructure-based mode; ATR-based mode; Tip-based mode; Fiber-based mode	Normal mode; Nanostructure-based mode; ATR-based mode	Normal mode; Nanostructure-based mode; ATR-based mode; Tip-based mode; Fiber-based mode
Detection sensitivity	High	High	Low[a]; Very high[c]
Surface selectivity	Low[a]; High[b]	Intrinsically high	Low[a]; High[b]
Applications	Electric double layer;[12,13,23,24,163–166] Electrocatalysis;[143,145,169–174] Rechargeable battery[118,159,185,186]	Electric double layer;[102,138–142] Electrocatalysis;[175–178] Rechargeable battery[187–189]	Electric double layer;[133–136,167,168] Electrocatalysis;[146,179–184] Rechargeable battery[154,190–193]
Advantages	Sensitive to *CO species, due to the high IR absorption cross-section of C–O bond; feasible to probe both the SEI and the electrolyte layer close to the surface; no interference by fluorescence background, etc.	Suitable for measurement on well-defined surface; intrinsic high surface selectivity and sensitivity in probing the orientation of surface species, e.g., molecular catalysts in heterogeneous electrocatalysis, etc.	Laser with a wavelength in visible region is feasible for operando experiments; no interference by H_2O and CO_2; suitable for the detection in low-frequency regions, e.g., the libration mode of water (<800 cm^{-1}), metal–carbon and/or metal–oxygen bonds, etc.
Challenges	Strong IR adsorption by H_2O and CO_2; possible interference from a window or prism (e.g., the interference in a low-frequency spectral region);influence of thin-layer electrolyte on electrochemistry, etc.	Strong IR adsorption by H_2O and CO_2; possible interference from a window or prism (e.g., the interference in a low-frequency spectral region); influence of a thin-layer electrolyte on electrochemical responses; smooth surface is desired, etc.	The cross-section of Raman scattering is very low; the surface-enhancement effect limits the generalities of surface morphology and electrode material; possible interference by a fluorescence background, etc.

[a] With a normal external reflection mode. [b] With nanostructure-, ATR-, or tip-based modes, the surface selectivity is high. [c] With a nanostructure-based mode, the detection sensitivity is up to a single-molecule level.[45]

This journal is © The Royal Society of Chemistry 2024

Chem. Soc. Rev., 2024, 53, 3579–3605 | 3597

through the closely packed solid layers, making it difficult to perform *operando* spectroscopic experiments in a traditional manner, *e.g.*, focusing the incident beam perpendicularly through the liquid electrolyte bulk to the electrode surface. As shown in Fig. 15, in the spectroelectrochemical study of a solid-state lithium–sulfur (Li–S) battery, the *operando* Raman cell with an open side was placed inside an inert argon environment to enable the spectroscopic detection of each battery component from the cross-sectional direction.[162] As revealed by the *operando* Raman spectra, sulfur (S_8, of which the Raman peaks are at 158, 220, and 473 cm^{-1}, respectively) underwent gradual reduction but was not completely reduced during the discharge process, while an intermediate species, that is, Li_2S_2 (438 cm^{-1}) appeared at the half charge state (2.359 V) and then disappeared at the full charge state (2.789 V), indicating that Li_2S was first oxidized to Li_2S_2, and then to S_8 during the charging process.[162] With a side opening cell, this method is suitable for the characterization of a solid-state electrolyte in *operando*, and thus to understand the emerging solid–solid electrochemical interfaces/interphases.

The development of electrochemical vibrational spectroscopy offers great opportunities for conducting *in situ* and *operando* studies in important areas such as fundamental electrochemistry, electrocatalysis, rechargeable batteries, *etc.* Each electrochemical vibrational spectroscopy technique (*i.e.*, EC-IR, EC-Raman, and EC-SFG) has advantages and limitations, which are briefly summarized in Table 2, and can be selected according to the practical requirements and applications.

4. Summary and outlook

4.1. Development trends

The application of *in situ* optical spectroscopy in electrochemistry was carried out six decades ago, with a significant growth since the 1990s, driven by advancements in nanoscience. The development of electrochemical optical spectroscopy, in particular vibrational spectroscopy, has made incalculable contribution not only to the progress of electrochemistry, but also to physical and chemical science and technology. It is foreseeable that electrochemical optical spectroscopy will be further innovated in both theory and experiments with the development of new spectroscopic techniques, instrumentation, nanotechnology, data-driven methods, *etc.*

The main development direction of electrochemical optical spectroscopy must be consistent with that of electrochemistry. Currently, electrochemical energy is of paramount importance in electrochemistry; therefore, it is desirable to further develop a new strategy, methodology, and research paradigm with respect to the different key scientific and technical problems in electrochemical energy studies.

For practical applications of electrochemical optical spectroscopy, the energy conversion and storage systems are in strong demand and facing the challenges of new systems with complex structures, raising unprecedented requirements for the capability of obtaining more reliable and useful

information of various electrochemical interfaces under working conditions, *i.e.*, developing *operando* spectroscopic methods with high detection sensitivity, along with high temporal and spatial resolutions. Furthermore, there are still great difficulties in *operando* studies under low and high temperature working conditions, *i.e.*, probing the emerging wide-temperature batteries for application under extreme climate/operation conditions.[194,195] It is imperative to develop new spectroscopic methods for characterization in such complex and extreme environments.

To discuss these significant explorations, examples illustratin the new strategies, methodologies, and research paradigm in electrochemical optical spectroscopy are presented below.

4.2. New strategies, methodologies, and research paradigms

4.2.1. New "borrowing" strategy in EC-SERS. In the *operando* EC-Raman study of an electrochemical energy device, the electrode materials are usually SERS-inactive or weakly SERS-inactive, such as cathode and anode materials in Li-ion batteries. As discussed in Section 2.2.2, an effective way to probe
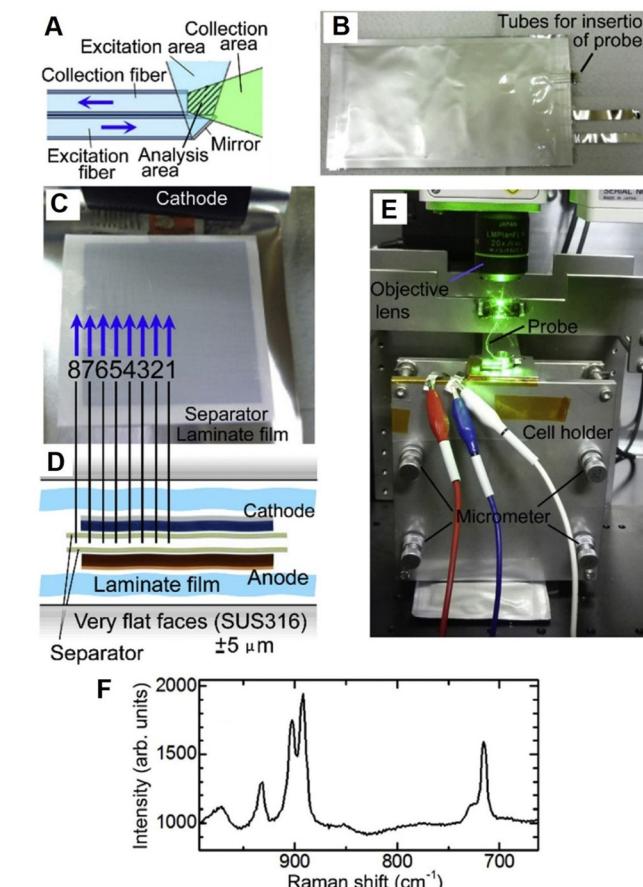
Fig. 16 (A)–(F) *Operando* Raman spectroscopic measurement inside a laminate cell using microprobes. (A) Schematic of probe consisting of one excitation optical fiber and one collection fiber. (B) Photograph of a laminate cell inserted with eight microprobes. (C) Inside and (D) cross-section view of the laminate cell with the probes. (E) Photograph of setup of the *operando* fiber-based Raman spectroscopic measurement. (F) Raman spectrum of electrolyte inside the laminate cell. Reproduced with permission from ref. 130. Copyright 2017 Elsevier B.V.

3598 | *Chem. Soc. Rev.*, 2024, **53**, 3579–3605

This journal is © The Royal Society of Chemistry 2024

the electrode materials with weak or no SERS-activity is to employ a strategy of "borrowing" SERS activity. In the conventional SHINERS method (Fig. 7), the ultrathin shell of SHIN can prevent the adsorption of the analyte on the Au core surface while allowing the "borrowing" of SERS activity from the Au core to boost the Raman signal from the probe material surface. However, the Raman enhancement of the analyte is limited because the electromagnetic field generated from the plasmonic Au core will be attenuated exponentially due to the presence of a dielectric shell (an electromagnetic field decrease of ∼5 times or more).[72] Hence, it is important to design new nanostructures to engineer the SERS hotspots, figuratively speaking, to push the hotspot outside the shell in the SHINERS method, and thus making it closer to the surface of probe material surface, which could further enhance the enhancement in the SHINERS method. Presumably, a method to achieve this goal is to use a shell material with a high-refractive index, such as Si, GaP, and TiO_2.[196,197] In these scenarios, the high-refractive index shell could serve as a "nanoscale lens" that is able to concentrate the field into the medium, and thus it could provide a much higher local electric enhancement on the surface of the dielectric shell.[106] Therefore, the hotspots are located on the outer shell surface of SHIN, leading to a much higher Raman enhancement of the analytes.

It is worth noting that SERS-active substrate materials have been expanded beyond "free-electron like" metals to the semiconductor/dielectric substrates[198] as well as graphene materials,[199] opening up new avenues for EC-SERS applications. In particular, the roles of such SERS-active substrates are manifold, e.g., graphene can simultaneously act as a Raman probe to reveal the spectroelectrochemical features of carbon materials.[200–202]

4.2.2. *Operando* fiber-based electrochemical vibrational spectroscopy. There is an urgent need to develop *operando* spectroscopic methods that have the advantages of a probe that does not interfere with the working conditions of an electrochemical device and be nondestructive.[203] In Li-ion batteries, the *in situ* or *operando* studies of EEIs are normally performed on the half cells using lithium foil as the counter (reference) electrode; however, the corresponding (electro)chemical behavior is different from that of a commercial full cell typically using a graphite anode. It is worth noting that the volume of electrolyte used in a half-cell testing system is generally smaller than that in the commercial cells, resulting in deviations in the study of the complex interaction between the electrode and electrolyte from those in a practical full battery.[131] Owing to the miniaturization and non-destructive properties, fiber optics is widely used for invasive analysis. By directly embedding fiber optic sensors within a practical battery and combining with vibrational spectroscopy, that is, fiber-based mode electrochemical vibrational spectroscopy (Fig. 4E), people are able to monitor Li-ion chemistry in a full battery in *operando*.[40,41,130,131]

As shown in Fig. 16A–F, Yamanaka *et al.* placed eight ultra-fine fiber Raman probes inside a practical laminate lithium-ion battery at different positions to monitor the electrolyte concentration variations.[130] The probe consists of two silica-based optical fibers, *i.e.*, one excitation fiber for laser light and one collection fiber for Raman signals, where the total cross-sectional area of the probe is around 30 μm × 60 μm.[40,130] Usually, the Raman spectroscopic measurement offers an averaged information of electrolyte from a battery. However, based on the ultra-fine spectroscopic probes at different locations inside the battery, the concentration gradient of electrolyte in the plane parallel to the electrode surfaces was observed and the corresponding changes during cycles were monitored in *operando*. Hence, this measurement will be beneficial for the studies of ion migration and related position-dependent reactions inside a battery.

Since silica-based fiber is typically limited to the spectral range from 0.8 to 2 μm, to enable to fiber-based spectroelectrochemistry in the IR range, chalcogenide glass fiber can be employed instead.[41] As shown by the schematic in Fig. 17A,
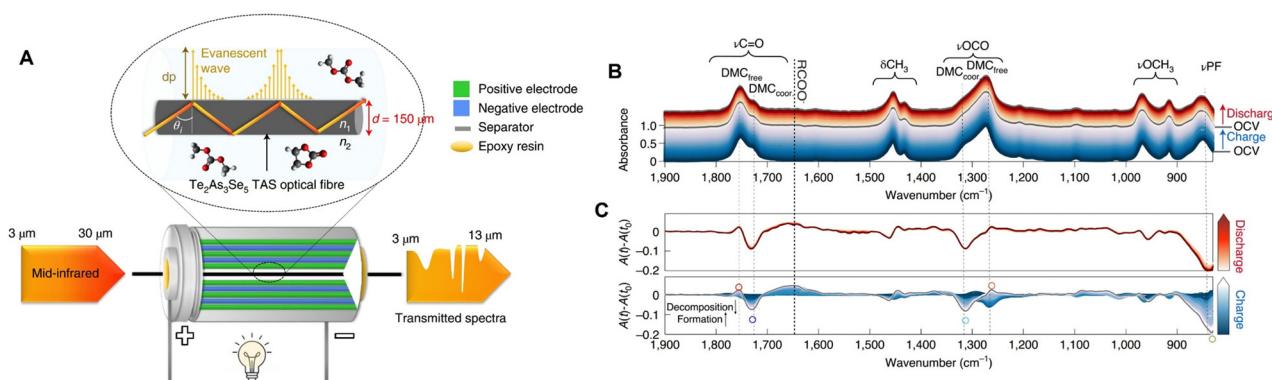
Fig. 17 (A) Schematic of *operando* IR fiber evanescent wave spectroscopy (FEWS) using mid-IR light in the range from 830 to 5000 cm^{-1} passing through the Te$_2$As$_3$Se$_5$ (TAS) fiber core (a diameter of 150 μm). The TAS fiber is located in the central void of a commercial 18650 jelly roll, allowing IR-FEWS measurements of the electrolyte under *operando* conditions. (B) *Operando* IR-FEWS spectra obtained during the first charge−discharge cycle. The spectra in charge were colored in blue, while those in discharge were colored in red. (C) The relative IR absorbance changes ($A(t) - A(t_0)$) obtained in charge (bottom) and discharge (top). Reproduced with permission from ref. 41. Copyright 2022 Springer Nature.

This journal is © The Royal Society of Chemistry 2024

Chem. Soc. Rev., 2024, **53**, 3579–3605 | **3599**

incident light source. In this regard, the powerful free electron laser (FEL) technology is capable of fully tunable wavelength, high-quality light beam, high-level polarization, high peak brightness, and high average power, *etc.*[209] Therefore, the application of FEL will be definitely beneficial for progress of spectroelectrochemistry.[6]

4.2.4. Electrochemical optical spectroscopy for synthetic electrochemistry. In October 2023, the International Union of Pure and Applied Chemistry (IUPAC) announced that synthetic electrochemistry has been selected as one of the top ten emerging technologies in chemistry due to its significant potential in promoting global sustainability.[210] In this field, electrochemistry offers an economical and environmentally friendly way to tailor the synthetic processes with a high level of chemo- and regio-selectivity.[211] Typically, the electrochemical measurement, such as CV, is used to elucidate the electrochemical synthetic mechanisms.[212] However, for some complex synthesis processes involving both chemical and electrochemical reactions, it is essential to introduce optical spectroscopy with molecular recognition capability to *in situ* analyze yields and reaction selectivity in a comprehensive and sensitive manner.

Compared to vibrational spectroscopy, EC-UV-Vis spectroscopy has advantages in sensitivity and quantitative analytical capability for the study of electrolyte bulk; it has widely contributed to the *in situ* characterization of electrogenerated species and study of redox processes.[213,214] Thus, EC-UV-Vis is suitable for the quantitative analysis of large number of intermediates during electrochemical synthesis.

The reversible chemical/electrochemical interconversion between quinone and hydroquinone has been widely recognized in electrochemical synthesis and organic redox flow batteries.[215,216] Recently, it was used in a nickel-catalyzed cross-electrophile coupling (XEC) reaction to synthesize pharmaceutical intermediates on a hectogram scale (100 g scale).[215] In this work, nickel-catalyzed XEC reaction was supported by a quinone-mediated H_2 anode under non-aqueous conditions. UV-Vis spectroscopy was employed to *in situ* investigate the interplay between thermal catalytic hydrogenation of sodium anthraquinone-2-sulfonate (AQS) and the electrochemical oxidation of the corresponding anthrahydroquinone ($AQSH_2$) in real time. As shown in Fig. 18, the redox speciation of AQS (with an absorption band at $\sim$330 nm) and $AQSH_2$ (with an adsorption band at $\sim$380 nm) species in the anolyte reservoir was studied using UV-Vis spectroscopy during various processes, such as hydrogenation-only or electrolysis-only loop, or both loops operating simultaneously. This spectroelectrochemical method demonstrates significant potential in the real-time analysis for the development of highly-efficient, large-scale synthetic electrochemistry.

After sixty years of development and growth, electrochemical optical spectroscopy has become one of the most important branches of spectroelectrochemistry. Based on the promising development trend, we are optimistic that in the near future, the emergence of new breakthroughs in spectroelectrochemistry will bring incalculable impact not only to the progress of

electrochemistry, but also on surface/interface science and the wider fields of materials science and technology.

Conflicts of interest

The authors declare no conflicts of interest.

Acknowledgements

Notes and references

1 J. O. 'M. Bockris and K. Khan, *Surface Electrochemistry*, Plenum, New York, 1993.
2 H. D. Abruña, *Electrochemical Interfaces—Modern Techniques for in-situ Interface Characterization*, VCH, Berlin, 1991.
3 J. Lipkowski and P. N. Ross, *Adsorption at Electrode Surface*, VCH, New York, 1992.
4 A. J. Bard and L. R. Faulkner, *Electrochemical Methods: Fundamentals and Applications*, Wiley, New York, 2000.
5 *In-situ Spectroscopic Studies of Adsorption at the Electrode and Electrocatalysis*, ed. S.-G. Sun, P. A. Christensen and A. Wieckowski, Elsevier Science B.V., Amsterdam, 2007.
6 Z.-Q. Tian, *et al.*, *Spectro-electrochemistry*, Chemical Industry Press Co., Ltd., Beijing, 2021.
7 A. K. N. Reddy, M. A. V. Devanathan and J. O. 'M. Bockris, *J. Electroanal. Chem.*, 1963, **6**, 61–67.
8 T. Kuwana, R. K. Darlington and D. W. Leedy, *Anal. Chem.*, 1964, **36**, 2023–2025.
9 H. B. Mark and B. S. Pons, *Anal. Chem.*, 1966, **38**, 119–121.
10 C. H. Lee, R. K. Chang and N. Bloembergen, *Phys. Rev. Lett.*, 1967, **18**, 167–170.
11 M. Fleischmann, P. J. Hendra and A. J. McQuillan, *J. Chem. Soc., Chem. Commun.*, 1973, 80–81.
12 A. Bewick, K. Kunimatsu and B. Stanley Pons, *Electrochim. Acta*, 1980, **25**, 465–468.
13 A. Bewick and K. Kunimatsu, *Surf. Sci.*, 1980, **101**, 131–138.
14 P. Guyot-Sionnest and A. Tadjeddine, *Chem. Phys. Lett.*, 1990, **172**, 341–345.
15 M. Fleischmann, P. J. Hendra and A. J. McQuillan, *Chem. Phys. Lett.*, 1974, **26**, 163–166.
16 D. L. Jeanmaire and R. P. Van Duyne, *J. Electroanal. Chem. Interfacial Electrochem.*, 1977, **84**, 1–20.
17 M. Fleischmann, Z. Q. Tian and L. J. Li, *J. Electroanal. Chem. Interfacial Electrochem.*, 1987, **217**, 397–410.
18 L. W. H. Leung and M. J. Weaver, *J. Am. Chem. Soc.*, 1987, **109**, 5113–5119.
19 L.-W. H. Leung and M. J. Weaver, *J. Electroanal. Chem. Interfacial Electrochem.*, 1987, **217**, 367–384.

This journal is © The Royal Society of Chemistry 2024

Chem. Soc. Rev., 2024, **53**, 3579–3605 | 3601

20 G. Mengoli, M. M. Musiani, M. Fleischman, B. Mao and Z. Q. Tian, *Electrochim. Acta*, 1987, **32**, 1239–1245.

21 R. G. Freeman, K. C. Grabar, K. J. Allison, R. M. Bright, J. A. Davis, A. P. Guthrie, M. B. Hommer, M. A. Jackson, P. C. Smith, D. G. Walter and M. J. Natan, *Science*, 1995, **267**, 1629–1632.

22 M. Osawa, K.-i Ataka, K. Yoshii and T. Yotsuyanagi, *J. Electron Spectros. Relat. Phenomena*, 1993, **64–65**, 371–379.

23 K.-i Ataka, T. Yotsuyanagi and M. Osawa, *J. Phys. Chem.*, 1996, **100**, 10664–10672.

24 K.-i Ataka and M. Osawa, *Langmuir*, 1998, **14**, 951–959.

25 W.-B. Cai, L.-J. Wan, H. Noda, Y. Hibino, K. Ataka and M. Osawa, *Langmuir*, 1998, **14**, 6992–6998.

26 F. Kitamura, M. Takeda, M. Takahashi and M. Ito, *Chem. Phys. Lett.*, 1987, **142**, 318–322.

27 F. Kitamura, M. Takahashi and M. Ito, *J. Phys. Chem.*, 1988, **92**, 3320–3323.

28 R. J. Nichols and A. Bewick, *J. Electroanal. Chem. Interfacial Electrochem.*, 1988, **243**, 445–453.

29 S. P. Byahut and T. E. Furtak, *Electrochim. Acta*, 1991, **36**, 1879–1882.

30 A. Bruckbauer and A. Otto, *J. Raman Spectrosc.*, 1998, **29**, 665–672.

31 A. Peremans and A. Tadjeddine, *Phys. Rev. Lett.*, 1994, **73**, 3010–3013.

32 W. Daum, K. A. Friedrich, C. Klünker, D. Knabben, U. Stimming and H. Ibach, *Appl. Phys. A*, 1994, **59**, 553–562.

33 J. F. Li, Y. F. Huang, Y. Ding, Z. L. Yang, S. B. Li, X. S. Zhou, F. R. Fan, W. Zhang, Z. Y. Zhou, D. Y. Wu, B. Ren, Z. L. Wang and Z. Q. Tian, *Nature*, 2010, **464**, 392–395.

34 Z.-C. Zeng, S.-C. Huang, D.-Y. Wu, L.-Y. Meng, M.-H. Li, T.-X. Huang, J.-H. Zhong, X. Wang, Z.-L. Yang and B. Ren, *J. Am. Chem. Soc.*, 2015, **137**, 11928–11931.

35 D. Kurouski, M. Mattei and R. P. Van Duyne, *Nano Lett.*, 2015, **15**, 7956–7962.

36 Y.-H. Lu, J. M. Larson, A. Baskin, X. Zhao, P. D. Ashby, D. Prendergast, H. A. Bechtel, R. Kostecki and M. Salmeron, *Nano Lett.*, 2019, **19**, 5388–5393.

37 I. Kendrick, D. Kumari, A. Yakaboski, N. Dimakis and E. S. Smotkin, *J. Am. Chem. Soc.*, 2010, **132**, 17611–17616.

38 M. Hara, J. Inukai, K. Miyatake, H. Uchida and M. Watanabe, *Electrochim. Acta*, 2011, **58**, 449–455.

39 P. Huguet, A. Morin, G. Gebel, S. Deabate, A. K. Sutor and Z. Peng, *Electrochem. Commun.*, 2011, **13**, 418–422.

40 T. Yamanaka, H. Nakagawa, M. Ochida, S. Tsubouchi, Y. Domi, T. Doi, T. Abe and Z. Ogumi, *J. Phys. Chem. C*, 2016, **120**, 2585–2591.

41 C. Gervillié-Mouravieff, C. Boussard-Plédel, J. Huang, C. Leau, L. A. Blanquer, M. B. Yahia, M. L. Doublet, S. T. Boles, X. H. Zhang, J. L. Adam and J. M. Tarascon, *Nat. Energy*, 2022, **7**, 1157–1169.

42 I. Bergman, B. E. Conway, A. Bewick, T. Kuwana, J. D. E. McIntyre, C. L. Gardner, E. J. Casey, M. A. Barrett, H. Angerstein-Kozlowska, D. M. Kolb, M. Keddam, A. J. McQuillan, J. S. Clarke, A. T. Kuhn and W. J. Orville-Thomas, *Faraday Spec. Discuss. Chem. Soc.*, 1973, **56**, 152–170.

43 J. W. Strojek and T. Kuwana, *J. Electroanal. Chem.*, 1968, **16**(4), 471–483.

44 P. J. Hendra, *Int. J. Vib. Spect.*, 2000, **4**, 1.

45 Z.-Q. Tian and B. Ren, *Encyclopedia of Electrochemistry*, Wiley-VCH, 2007, ch. 6, pp. 572–659.

46 M. R. Anderson and C. D. Taylor, *Encyclopedia of Analytical Chemistry*, 2007.

47 Y. R. Shen, *Nature*, 1989, **337**, 519–525.

48 G. A. Somorjai and Y. Li, *Introduction to surface chemistry and catalysis*, John Wiley & Sons, 2010.

49 Z.-Q. Tian and B. Ren, *Annu. Rev. Phys. Chem.*, 2004, **55**, 197–229.

50 Z.-Q. Tian, B. Ren and D.-Y. Wu, *J. Phys. Chem. B*, 2002, **106**, 9463–9483.

51 A. Bewick, K. Kunimatsu, B. S. Pons and J. W. Russell, *J. Electroanal. Chem. Interfacial Electrochem.*, 1984, **160**, 47–61.

52 Z.-Q. Tian and B. Ren, *Encyclopedia of Analytical Chemistry*, John Wiley & Sons, Ltd, 2006.

53 A. Tadjeddine and F. Vidal, *In-situ Spectroscopic Studies of Adsorption at the Electrode and Electrocatalysis*, ed. S.-G. Sun, P. A. Christensen and A. Wieckowski, Elsevier Science B.V., Amsterdam, 2007, pp. 273–298.

54 A. McClelland and Z. Chen, *Encyclopedia of Analytical Chemistry*, John Wiley & Sons, Ltd., 2008.

55 S. Ye and K. Uosaki, in *Encyclopedia of Electrochemistry*, ed. A. J. Bard and M. Stratmann, Wiley-VCH Verlag GmbH, Weinheim, 2007, vol. 10, pp. 513–553.

56 A. Ge, K.-i Inoue and S. Ye, *J. Chem. Phys.*, 2020, **153**, 170902.

57 J. H. Hunt, P. Guyot-Sionnest and Y. R. Shen, *Chem. Phys. Lett.*, 1987, **133**, 189–192.

58 X. D. Zhu, H. Suhr and Y. R. Shen, *Phys. Rev. B: Condens. Matter Mater. Phys.*, 1987, **35**, 3047–3050.

59 P. Guyot-Sionnest, J. H. Hunt and Y. R. Shen, *Phys. Rev. Lett.*, 1987, **59**, 1597–1600.

60 J.-F. Li, Y.-J. Zhang, S.-Y. Ding, R. Panneerselvam and Z.-Q. Tian, *Chem. Rev.*, 2017, **117**, 5002–5069.

61 M. Osawa, in *Near-Field Optics and Surface Plasmon Polaritons*, ed. S. Kawata, Springer Berlin Heidelberg, Berlin, Heidelberg, 2001, pp. 163–187.

62 M. G. Albrecht and J. A. Creighton, *J. Am. Chem. Soc.*, 1977, **99**, 5215–5217.

63 R. P. Van Duyne, in *Chemical and Biochemical Applications of Lasers*, ed. C. B. Moore, Academic Press, 1979, pp. 101–185.

64 R. K. Chang and T. E. Furtak, *Surface Enhanced Raman Scattering*, Plenum Press, New York, 1982.

65 M. Moskovits, *J. Raman Spectrosc.*, 2005, **36**, 485–496.

66 E. C. Le Ru and P. G. Etchegoin, in *Principles of Surface-Enhanced Raman Spectroscopy*, ed. E. C. Le Ru and P. G. Etchegoin, Elsevier, Amsterdam, 2009, pp. 121–183.

67 K. A. Willets and R. P. Van Duyne, *Annu. Rev. Phys. Chem.*, 2007, **58**, 267–297.

68 S. A. Maier, *Plasmonics: fundamentals and applications*, Springer, New York, 2007.

69 J. A. Creighton, C. G. Blatchford and M. G. Albrecht, *J. Chem. Soc., Faraday Trans. 2*, 1979, **75**, 790–798.

70 M. Moskovits, *J. Chem. Phys*, 1978, **69**, 4159–4161.

71 Z.-Q. Tian, B. Ren, J.-F. Li and Z.-L. Yang, *Chem. Commun.*, 2007, 3514–3534.

72 S.-Y. Ding, J. Yi, J.-F. Li, B. Ren, D.-Y. Wu, R. Panneerselvam and Z.-Q. Tian, *Nat. Rev. Mater.*, 2016, **1**, 16021.

73 R. P. Van Duyne and J. P. Haushalter, *J. Phys. Chem.*, 1983, **87**, 2999–3003.

74 S. Park, P. Yang, P. Corredor and M. J. Weaver, *J. Am. Chem. Soc.*, 2002, **124**, 2428–2429.

75 L. Lu, G. Sun, H. Zhang, H. Wang, S. Xi, J. Hu, Z. Tian and R. Chen, *J. Mater. Chem.*, 2004, **14**, 1005–1009.

76 J.-W. Hu, Y. Zhang, J.-F. Li, Z. Liu, B. Ren, S.-G. Sun, Z.-Q. Tian and T. Lian, *Chem. Phys. Lett.*, 2005, **408**, 354–359.

77 J.-F. Li, Z.-L. Yang, B. Ren, G.-K. Liu, P.-P. Fang, Y.-X. Jiang, D.-Y. Wu and Z.-Q. Tian, *Langmuir*, 2006, **22**, 10372–10379.

78 C. G. Blatchford, J. R. Campbell and J. A. Creighton, *Surf. Sci.*, 1982, **120**, 435–455.

79 C. L. Haynes and R. P. Van Duyne, *J. Phys. Chem. B*, 2001, **105**, 5599–5611.

80 L. A. Dick, A. D. McFarland, C. L. Haynes and R. P. Van Duyne, *J. Phys. Chem. B*, 2002, **106**, 853–860.

81 P. N. Bartlett, J. J. Baumberg, S. Coyle and M. E. Abdelsalam, *Faraday Discuss.*, 2004, **125**, 117–132.

82 S. Mahajan, M. Abdelsalam, Y. Suguwara, S. Cintra, A. Russell, J. Baumberg and P. Bartlett, *Phys. Chem. Chem. Phys.*, 2007, **9**, 104–109.

83 P. L. Stiles, J. A. Dieringer, N. C. Shah and R. P. V. Duyne, *Annu. Rev. Anal. Chem.*, 2008, **1**, 601–626.

84 A. Hartstein, J. R. Kirtley and J. C. Tsang, *Phys. Rev. Lett.*, 1980, **45**, 201–204.

85 A. Hatta, T. Ohshima and W. Suëtaka, *Appl. Phys. A*, 1982, **29**, 71–75.

86 A. Hatta, Y. Suzuki and W. Suëtaka, *Appl. Phys. A*, 1984, **35**, 135–140.

87 M. Osawa, *Bull. Chem. Soc. Jpn*, 1997, **70**, 2861–2880.

88 M. Osawa, M. Kuramitsu, A. Hatta, W. Suëtaka and H. Seki, *Surf. Sci.*, 1986, **175**, L787–L793.

89 M. Osawa, K.-I. Ataka, K. Yoshii and Y. Nishikawa, *Appl. Spectrosc.*, 1993, **47**, 1497–1502.

90 Y. Nishikawa, T. Nagasawa, K. Fujiwara and M. Osawa, *Vib. Spectrosc.*, 1993, **6**, 43–53.

91 P. A. Christensen, in *Encyclopedia of Electrochemistry*, 2007.

92 H.-L. Wang, E.-M. You, R. Panneerselvam, S.-Y. Ding and Z.-Q. Tian, *Light Sci. Appl.*, 2021, **10**, 161.

93 M. Osawa, in *In-situ Spectroscopic Studies of Adsorption at the Electrode and Electrocatalysis*, ed. S.-G. Sun, P. A. Christensen and A. Wieckowski, Elsevier Science B.V., Amsterdam, 2007, pp. 209–246.

94 G.-Q. Lu, S.-G. Sun, S.-P. Chen and L.-R. Cai, *J. Electroanal. Chem.*, 1997, **421**, 19–23.

95 G.-Q. Lu, S.-G. Sun, L.-R. Cai, S.-P. Chen, Z.-W. Tian and K.-K. Shiu, *Langmuir*, 2000, **16**, 778–786.

96 E. V. Alieva, L. A. Kuzik and V. A. Yakovlev, *Chem. Phys. Lett.*, 1998, **292**, 542–546.

97 E. W. M. van der Ham, Q. H. F. Vrehen, E. R. Eliel, V. A. Yakovlev, E. V. Alieva, L. A. Kuzik, J. E. Petrov, V. A. Sychugov and A. F. G. van der Meer, *J. Opt. Soc. Am. B*, 1999, **16**, 1146–1152.

98 S. Baldelli, A. S. Eppler, E. Anderson, Y.-R. Shen and G. A. Somorjai, *J. Chem. Phys.*, 2000, **113**, 5432–5438.

99 T. Kawai, D. J. Neivandt and P. B. Davies, *J. Am. Chem. Soc.*, 2000, **122**, 12031–12032.

100 Y. He, H. Ren, E.-M. You, P. M. Radjenovic, S.-G. Sun, Z.-Q. Tian, J.-F. Li and Z. Wang, *Phys. Rev. Lett.*, 2020, **125**, 047401.

101 Y. Yang, Y. Xiong, R. Zeng, X. Lu, M. Krumov, X. Huang, W. Xu, H. Wang, F. J. DiSalvo, J. D. Brock, D. A. Muller and H. D. Abruña, *ACS Catal.*, 2021, **11**, 1136–1178.

102 W.-T. Liu and Y. R. Shen, *Proc. Natl. Acad. Sci. U. S. A.*, 2014, **111**, 1293–1297.

103 C. Korzeniewski, in *In-situ Spectroscopic Studies of Adsorption at the Electrode and Electrocatalysis*, ed. S.-G. Sun, P. A. Christensen and A. Wieckowski, Elsevier Science B.V., Amsterdam, 2007, pp. 179–208.

104 N. Furuya, S. Motto and K. Kunimatsu, *J. Electroanal. Chem. Interfacial Electrochem.*, 1988, **239**, 347–360.

105 A. J. Wilson and K. A. Willets, *Nano Lett.*, 2014, **14**, 939–945.

106 C.-Y. Li, J. Yi, R. Hu, J.-F. Li and Z.-Q. Tian, in *Encyclopedia of Nanomaterials*, ed. Y. Yin, Y. Lu and Y. Xia, Elsevier, Oxford, 1st edn, 2023, vol. 1, pp. 511–535.

107 D. M. Kolb, *Angew. Chem., Int. Ed.*, 2001, **40**, 1162–1181.

108 O. M. Magnussen, *Chem. Rev.*, 2002, **102**, 679–726.

109 A. A. Gewirth and B. K. Niece, *Chem. Rev.*, 1997, **97**, 1129–1162.

110 Z. Q. Tian, W. H. Li, B. Ren, B. W. Mao, J. G. Chen, J. Q. Mu, X. D. Zhuo and D. Wang, *J. Electroanal. Chem.*, 1996, **401**, 247–251.

111 Z.-Q. Tian, W.-H. Li, J.-Q. Mu, B.-W. Mao, J.-G. Chen, X.-D. Zhuo, W. Zheng, D. Wang and E.-R. Yan, *Acta Phys. Chim.*, 1994, **10**, 1062–1065.

112 M. S. Anderson, *Appl. Phys. Lett.*, 2000, **76**, 3130–3132.

113 N. Hayazawa, Y. Inouye, Z. Sekkat and S. Kawata, *Opt. Commun.*, 2000, **183**, 333–336.

114 R. M. Stöckle, Y. D. Suh, V. Deckert and R. Zenobi, *Chem. Phys. Lett.*, 2000, **318**, 131–136.

115 B. Pettinger, G. Picardi, R. Schuster and G. Ertl, *Electrochemistry*, 2000, **68**, 942–949.

116 S.-C. Huang, X. Wang, Q.-Q. Zhao, J.-F. Zhu, C.-W. Li, Y.-H. He, S. Hu, M. M. Sartin, S. Yan and B. Ren, *Nat. Commun.*, 2020, **11**, 4211.

117 J. J. Schwartz, D. S. Jakob and A. Centrone, *Chem. Soc. Rev.*, 2022, **51**, 5248–5267.

118 X. He, J. M. Larson, H. A. Bechtel and R. Kostecki, *Nat. Commun.*, 2022, **13**, 1398.

119 S. Amemiya, A. J. Bard, F.-R. F. Fan, M. V. Mirkin and P. R. Unwin, *Annu. Rev. Anal. Chem.*, 2008, **1**, 95–131.

This journal is © The Royal Society of Chemistry 2024

Chem. Soc. Rev., 2024, **53**, 3579–3605 | 3603

120 C. L. Brosseau, A. Colina, J. V. Perales-Rondon, A. J. Wilson, P. B. Joshi, B. Ren and X. Wang, *Nat. Rev. Methods Primers*, 2023, **3**, 79.

121 W. Schuhmann, D. Öhl and D. M. Morales, in *Springer Handbook of Advanced Catalyst Characterization*, ed. I. E. Wachs and M. A. Bañares, Springer International Publishing, Cham, 2023, pp. 189–211.

122 J. Clausmeyer, M. Nebel, S. Grützke, Y. U. Kayran and W. Schuhmann, *ChemPlusChem*, 2018, **83**, 414–417.

123 K. O. Hatfield, M. T. Gole, N. B. Schorr, C. J. Murphy and J. Rodríguez-López, *Anal. Chem.*, 2021, **93**, 7792–7796.

124 M. A. Bañares and I. E. Wachs, *J. Raman Spectrosc.*, 2002, **33**, 359–380.

125 A. Gurlo and R. Riedel, *Angew. Chem., Int. Ed.*, 2007, **46**, 3826–3848.

126 B. M. Weckhuysen, *Chem. Commun.*, 2002, 97–110.

127 A. M. Tripathi, W.-N. Su and B. J. Hwang, *Chem. Soc. Rev.*, 2018, **47**, 736–851.

128 J. Tan, D. Liu, X. Xu and L. Mai, *Nanoscale*, 2017, **9**, 19001–19016.

129 L. Meyer, N. Saqib and J. Porter, *J. Electrochem. Soc.*, 2021, **168**, 090561.

130 T. Yamanaka, H. Nakagawa, S. Tsubouchi, Y. Domi, T. Doi, T. Abe and Z. Ogumi, *J. Power Sources*, 2017, **359**, 435–440.

131 E. Miele, W. M. Dose, I. Manyakin, M. H. Frosz, Z. Ruff, M. F. L. De Volder, C. P. Grey, J. J. Baumberg and T. G. Euser, *Nat. Commun.*, 2022, **13**, 1651.

132 T. Lombardo, M. Duquesnoy, H. El-Bouysidy, F. Åérn, A. Gallo-Bueno, P. B. Jørgensen, A. Bhowmik, A. Demortière, E. Ayerbe, F. Alcaide, M. Reynaud, J. Carrasco, A. Grimaud, C. Zhang, T. Vegge, P. Johansson and A. A. Franco, *Chem. Rev.*, 2022, **122**, 10899–10969.

133 M. Fleischmann, P. J. Hendra, I. R. Hill and M. E. Pemble, *J. Electroanal. Chem. Interfacial Electrochem.*, 1981, **117**, 243–255.

134 C.-Y. Li, J.-B. Le, S. Chen, Z.-L. Yang, J.-F. Li, J. Cheng and Z.-Q. Tian, *Nat. Mater.*, 2019, **18**, 697–701.

135 Y.-H. Wang, S. Zheng, W.-M. Yang, R.-Y. Zhou, Q.-F. He, P. Radjenovic, J.-C. Dong, S. Li, J. Zheng, Z.-L. Yang, G. Attard, F. Pan, Z.-Q. Tian and J.-F. Li, *Nature*, 2021, **600**, 81–85.

136 C.-Y. Li, M. Chen, S. Liu, X. Lu, J. Meng, J. Yan, H. D. Abruña, G. Feng and T. Lian, *Nat. Commun.*, 2022, **13**, 5330.

137 G. Gonella, E. H. G. Backus, Y. Nagata, D. J. Bonthuis, P. Loche, A. Schlaich, R. R. Netz, A. Kühnle, I. T. McCrum, M. T. M. Koper, M. Wolf, B. Winter, G. Meijer, R. K. Campen and M. Bonn, *Nat. Rev. Chem.*, 2021, **5**, 466–485.

138 Y. Tong, I. Y. Zhang and R. K. Campen, *Nat. Commun.*, 2018, **9**, 1313.

139 Y. Tong, F. Lapointe, M. Thämer, M. Wolf and R. K. Campen, *Angew. Chem., Int. Ed.*, 2017, **56**, 4211–4214.

140 A. Montenegro, C. Dutta, M. Mammetkuliev, H. Shi, B. Hou, D. Bhattacharyya, B. Zhao, S. B. Cronin and A. V. Benderskii, *Nature*, 2021, **594**, 62–65.

141 Z. D. Schultz, S. K. Shaw and A. A. Gewirth, *J. Am. Chem. Soc.*, 2005, **127**, 15916–15922.

142 S. Nihonyanagi, S. Ye, K. Uosaki, L. Dreesen, C. Humbert, P. Thiry and A. Peremans, *Surf. Sci.*, 2004, **573**, 11–16.

143 Y. X. Chen, A. Miki, S. Ye, H. Sakai and M. Osawa, *J. Am. Chem. Soc.*, 2003, **125**, 3680–3681.

144 Y. Hori, in *Modern Aspects of Electrochemistry*, ed. C. G. Vayenas, R. E. White and M. E. Gamboa-Aldeco, Springer New York, New York, NY, 2008, pp. 89–189.

145 S. Zhu, B. Jiang, W.-B. Cai and M. Shao, *J. Am. Chem. Soc.*, 2017, **139**, 15664–15667.

146 J.-C. Dong, X.-G. Zhang, V. Briega-Martos, X. Jin, J. Yang, S. Chen, Z.-L. Yang, D.-Y. Wu, J. M. Feliu, C. T. Williams, Z.-Q. Tian and J.-F. Li, *Nat. Energy*, 2019, **4**, 60–67.

147 J. Li and J. Gong, *Energy Environ. Sci.*, 2020, **13**, 3748–3779.

148 J. Pu, C. Zhong, J. Liu, Z. Wang and D. Chao, *Energy Environ. Sci.*, 2021, **14**, 3872–3911.

149 D. Atkins, E. Capria, K. Edström, T. Famprikis, A. Grimaud, Q. Jacquet, M. Johnson, A. Matic, P. Norby, H. Reichert, J.-P. Rueff, C. Villevieille, M. Wagemaker and S. Lyonnard, *Adv. Energy Mater.*, 2022, **12**, 2102694.

150 X. Cao, H. Li, Y. Qiao, M. Jia, X. Li, J. Cabana and H. Zhou, *Adv. Mater.*, 2021, **33**, 2004280.

151 A. Grimaud, W. T. Hong, Y. Shao-Horn and J. M. Tarascon, *Nat. Mater.*, 2016, **15**, 121–126.

152 B. Qiu, M. Zhang, Y. Xia, Z. Liu and Y. S. Meng, *Chem. Mater.*, 2017, **29**, 908–915.

153 Y. Qiao, S. Guo, K. Zhu, P. Liu, X. Li, K. Jiang, C.-J. Sun, M. Chen and H. Zhou, *Energy Environ. Sci.*, 2018, **11**, 299–305.

154 Y. Qiao, J. Yi, S. Wu, Y. Liu, S. Yang, P. He and H. Zhou, *Joule*, 2017, **1**, 359–370.

155 C.-Y. Li, J.-C. Dong, X. Jin, S. Chen, R. Panneerselvam, A. V. Rudnev, Z.-L. Yang, J.-F. Li, T. Wandlowski and Z.-Q. Tian, *J. Am. Chem. Soc.*, 2015, **137**, 7648–7651.

156 M. Gauthier, T. J. Carney, A. Grimaud, L. Giordano, N. Pour, H.-H. Chang, D. P. Fenning, S. F. Lux, O. Paschos, C. Bauer, F. Maglia, S. Lupart, P. Lamp and Y. Shao-Horn, *J. Phys. Chem. Lett.*, 2015, **6**, 4653–4672.

157 X. Shan, U. Patel, S. Wang, R. Iglesias and N. Tao, *Science*, 2010, **327**, 1363–1366.

158 M. Kitta, K. Murai, K. Yoshii and H. Sano, *J. Am. Chem. Soc.*, 2021, **143**, 11160–11170.

159 Y. Zhang, Y. Katayama, R. Tatara, L. Giordano, Y. Yu, D. Fraggedakis, J. G. Sun, F. Maglia, R. Jung, M. Z. Bazant and Y. Shao-Horn, *Energy Environ. Sci.*, 2020, **13**, 183–199.

160 J. Janek and W. G. Zeier, *Nat. Energy*, 2023, **8**, 230–240.

161 M. B. Dixit, J.-S. Park, P. Kenesei, J. Almer and K. B. Hatzell, *Energy Environ. Sci.*, 2021, **14**, 4672–4711.

162 D. Cao, X. Sun, F. Li, S.-M. Bak, T. Ji, M. Geiwitz, K. S. Burch, Y. Du, G. Yang and H. Zhu, *Angew. Chem., Int. Ed.*, 2023, **62**, e202302363.

163 A. Yamakata and M. Osawa, *J. Am. Chem. Soc.*, 2009, **131**, 6892–6893.

164 Y.-J. Zhang, Z.-F. Su, J.-F. Li and J. Lipkowski, *J. Phys. Chem. C*, 2020, **124**, 13240–13248.

3604 | *Chem. Soc. Rev.*, 2024, **53**, 3579–3605

This journal is © The Royal Society of Chemistry 2024

165 A. E. Russell, A. S. Lin and W. E. O'Grady, *J. Chem. Soc. Faraday Trans.*, 1993, **89**, 195–198.

166 M. A. Habib and J. O. Bockris, *Langmuir*, 1986, **2**, 388–392.

167 Z. Q. Tian, Y. X. Chen, B. W. Mao, C. Z. Li, J. Wang and Z. F. Liu, *Chem. Phys. Lett.*, 1995, **240**, 224–229.

168 Y.-X. Chen and A. Otto, *J. Raman Spectrosc.*, 2005, **36**, 736–747.

169 A. Cuesta, G. Cabello, C. Gutiérrez and M. Osawa, *Phys. Chem. Chem. Phys.*, 2011, **13**, 20091–20095.

170 C. T. Williams, C. G. Takoudis and M. J. Weaver, *J. Phys. Chem. B*, 1998, **102**, 406–416.

171 X. Chang, S. Vijay, Y. Zhao, N. J. Oliveira, K. Chan and B. Xu, *Nat. Commun.*, 2022, **13**, 2656.

172 M.-H. Shao, P. Liu and R. R. Adzic, *J. Am. Chem. Soc.*, 2006, **128**, 7408–7409.

173 Z. Su, M. Karaskiewicz, J. Rogalski, R. Bilewicz and J. Lipkowski, *J. Electroanal. Chem.*, 2020, **875**, 113820.

174 I. A. Cechanaviciute, R. P. Antony, O. A. Krysiak, T. Quast, S. Dieckhöfer, S. Saddeler, P. Telaar, Y.-T. Chen, M. Muhler and W. Schuhmann, *Angew. Chem., Int. Ed.*, 2023, **62**, e202218493.

175 R. L. Behrens, A. Lagutchev, D. D. Dlott and A. Wieckowski, *J. Electroanal. Chem.*, 2010, **649**, 32–36.

176 N. García Rey and D. D. Dlott, *J. Phys. Chem. C*, 2015, **119**, 20892–20899.

177 M. L. Clark, A. Ge, P. E. Videla, B. Rudshteyn, C. J. Miller, J. Song, V. S. Batista, T. Lian and C. P. Kubiak, *J. Am. Chem. Soc.*, 2018, **140**, 17643–17655.

178 F. Vidal, B. Busson, C. Six, O. Pluchery and A. Tadjeddine, *Surf. Sci.*, 2002, **502–503**, 485–489.

179 B. Ren, X. Q. Li, C. X. She, D. Y. Wu and Z. Q. Tian, *Electrochim. Acta*, 2000, **46**, 193–205.

180 H. Yang, Y. Yang and S. Zou, *J. Phys. Chem. C*, 2007, **111**, 19058–19065.

181 Y. Zhao, X.-G. Zhang, N. Bodappa, W.-M. Yang, Q. Liang, P. M. Radjenovica, Y.-H. Wang, Y.-J. Zhang, J.-C. Dong, Z.-Q. Tian and J.-F. Li, *Energy Environ. Sci.*, 2022, **15**, 3968–3977.

182 Y. Zhao, X. Chang, A. S. Malkani, X. Yang, L. Thompson, F. Jiao and B. Xu, *J. Am. Chem. Soc.*, 2020, **142**, 9735–9743.

183 T. A. Galloway and L. J. Hardwick, *J. Phys. Chem. Lett.*, 2016, **7**, 2119–2124.

184 Y.-H. Wang, J.-B. Le, W.-Q. Li, J. Wei, P. M. Radjenovic, H. Zhang, X.-S. Zhou, J. Cheng, Z.-Q. Tian and J.-F. Li, *Angew. Chem., Int. Ed.*, 2019, **58**, 16062–16066.

185 J.-T. Li, S.-R. Chen, F.-S. Ke, G.-Z. Wei, L. Huang and S.-G. Sun, *J. Electroanal. Chem.*, 2010, **649**, 171–176.

186 S.-I. Pyun and Y.-G. Ryu, *J. Electroanal. Chem.*, 1998, **455**, 11–17.

187 Q. Peng, J. Chen, H. Ji, A. Morita and S. Ye, *J. Am. Chem. Soc.*, 2018, **140**, 15568–15571.

188 Z. Peng, S. A. Freunberger, Y. Chen and P. G. Bruce, *Science*, 2012, **337**, 563–566.

189 A. Ge, D. Zhou, K.-I. Inoue, Y. Chen and S. Ye, *J. Phys. Chem. C*, 2020, **124**, 17538–17547.

190 C.-Y. Li, Y. Yu, C. Wang, Y. Zhang, S.-Y. Zheng, J.-F. Li, F. Maglia, R. Jung, Z.-Q. Tian and Y. Shao-Horn, *J. Phys. Chem. C*, 2020, **124**, 4024–4031.

191 T. A. Galloway, L. Cabo-Fernandez, I. M. Aldous, F. Braga and L. J. Hardwick, *Faraday Discuss.*, 2017, **205**, 469–490.

192 S. Hy, Felix, Y.-H. Chen, J.-Y. Liu, J. Rick and B.-J. Hwang, *J. Power Sources*, 2014, **256**, 324–328.

193 L. Johnson, C. Li, Z. Liu, Y. Chen, S. A. Freunberger, P. C. Ashok, B. B. Praveen, K. Dholakia, J.-M. Tarascon and P. G. Bruce, *Nat. Chem.*, 2014, **6**, 1091–1099.

194 J. Xu, J. Zhang, T. P. Pollard, Q. Li, S. Tan, S. Hou, H. Wan, F. Chen, H. He, E. Hu, K. Xu, X.-Q. Yang, O. Borodin and C. Wang, *Nature*, 2023, **614**, 694–700.

195 Y. Feng, L. Zhou, H. Ma, Z. Wu, Q. Zhao, H. Li, K. Zhang and J. Chen, *Energy Environ. Sci.*, 2022, **15**, 1711–1759.

196 S.-Y. Ding, E.-M. You, J. Yi, J.-F. Li and Z.-Q. Tian, *Faraday Discuss.*, 2017, **205**, 457–468.

197 L. Deng, Y. Zhai, Y. Chen, N. Wang and Y. Huang, *J. Phys. D: Appl. Phys.*, 2019, **52**, 43LT01.

198 I. Alessandri and J. R. Lombardi, *Chem. Rev.*, 2016, **116**, 14921–14981.

199 X. Ling, L. Xie, Y. Fang, H. Xu, H. Zhang, J. Kong, M. S. Dresselhaus, J. Zhang and Z. Liu, *Nano Lett.*, 2010, **10**, 553–561.

200 M. Kalbac, H. Farhat, J. Kong, P. Janda, L. Kavan and M. S. Dresselhaus, *Nano Lett.*, 2011, **11**, 1957–1963.

201 L. Kavan and L. Dunsch, *ChemPhysChem*, 2007, **8**, 974–998.

202 W. Xu, N. Mao and J. Zhang, *Small*, 2013, **9**, 1206–1224.

203 C. P. Grey and J. M. Tarascon, *Nat. Mater.*, 2017, **16**, 45–56.

204 C. Shi, W. Zhang, R. L. Birke and J. R. Lombardi, *J. Phys. Chem.*, 1990, **94**, 4766–4769.

205 C. Shi, W. Zhang, J. R. Lombardi and R. L. Birke, *J. Phys. Chem.*, 1992, **96**, 10093–10096.

206 C. Zong, C.-J. Chen, M. Zhang, D.-Y. Wu and B. Ren, *J. Am. Chem. Soc.*, 2015, **137**, 11768–11774.

207 C. Fang, R. R. Frontiera, R. Tran and R. A. Mathies, *Nature*, 2009, **462**, 200–204.

208 R. R. Frontiera, A.-I. Henry, N. L. Gruenke and R. P. Van Duyne, *J. Phys. Chem. Lett.*, 2011, **2**, 1199–1203.

209 K.-J. Kim, Z. Huang and R. Lindberg, *Synchrotron Radiation and Free-Electron Lasers: Principles of Coherent X-Ray Generation*, Cambridge University Press, Cambridge, 2017.

210 F. Gomollón-Bel, *Chem. Int.*, 2023, **45**, 14–22.

211 C. Kingston, M. D. Palkowitz, Y. Takahira, J. C. Vantourout, B. K. Peters, Y. Kawamata and P. S. Baran, *Acc. Chem. Res.*, 2020, **53**, 72–83.

212 M. C. Leech and K. Lam, *Nat. Rev. Chem.*, 2022, **6**, 275–286.

213 D. Zhang, R. Wang, X. Wang and Y. Gogotsi, *Nat. Energy*, 2023, **8**, 567–576.

214 K. J. Lee, N. Elgrishi, B. Kandemir and J. L. Dempsey, *Nat. Rev. Chem.*, 2017, **1**, 0039.

215 J. Twilton, M. R. Johnson, V. Sidana, M. C. Franke, C. Bottecchia, D. Lehnherr, F. Lévesque, S. M. M. Knapp, L. Wang, J. B. Gerken, C. M. Hong, T. P. Vickery, M. D. Weisel, N. A. Strotman, D. J. Weix, T. W. Root and S. S. Stahl, *Nature*, 2023, **623**, 71–76.

216 D. G. Kwabi, Y. Ji and M. J. Aziz, *Chem. Rev.*, 2020, **120**, 6467–6489.

This journal is © The Royal Society of Chemistry 2024

Chem. Soc. Rev., 2024, **53**, 3579–3605 | 3605